Biomass and Carbon Stocks Mapping Using LiDAR Data and Field Observations: The Case of Olive Groves on Lesvos Island, Greece

By

Elena Palenova

Submitted to

Central European University

Department of Environmental Sciences and Policy

In partial fulfilment of the requirements for the Erasmus Mundus Joint Master Degree in Environmental Sciences, Policy, and Management (MESPOM)

Supervisor: Professor Themistoklis Kontos

Department of Environment, University of the Aegean

Vienna, Austria

2021

Notes on copyright and the ownership of intellectual property rights

(3) For bibliographic and reference purposes this thesis should be referred to as:

Palenova, E. 2021. *Biomass and carbon stocks mapping using LiDAR data and field observations: the case of olive groves on Lesvos island, Greece*. Thesis for the Erasmus Mundus Joint Master Degree in Environmental Sciences, Policy and Management programme, Central European University, Vienna.

Further information on the conditions under which disclosures and exploitation may take place is available from the Head of the Department of Environmental Sciences and Policy, Central European University.

Author's declaration

No portion of the work referred to in this thesis has been submitted in support of an application for another degree or qualification of this or any other university or other institutes of learning.

Elena PALENOVA

CENTRAL EUROPEAN UNIVERSITY

ABSTRACT OF THESIS submitted by:

Elena PALENOVA

in fulfillment of the Master of Science degree awarded as a result of successful completion of the Erasmus Mundus Masters course in Environmental Sciences, Policy and Management (MESPOM) jointly operated by the University of the Aegean, Central European University, Lund University, and the University of Manchester

and entitled: Biomass and Carbon Stocks Mapping Using LiDAR Data and Field Observations: The Case of Olive Groves on Lesvos Island, Greece.

Month and year of submission: June 2021

Abstract

Accessing and mapping aboveground biomass (AGB) is crucial for understanding the global carbon cycle. Agricultural lands are providing carbon storage as an additional ecosystem service. Remotely sensed data can be used to estimate and monitor carbon stored in agricultural plantations. LiDAR data, Satellite Images, and field observations can be used for obtaining detailed information about carbon stocks on the local and global levels. Such parameters and Leaf and Plant Area index were retrieved from field data and NASA's GEDI product L2B, used for calculating AGB and tested for correlation with Landsat 8 bands and vegetation indices. The research showed the potential of using data retrieved from GEDI for assessing and mapping AGB and carbon stocks of olive groves on Lesvos Island, Greece. Maps on AGB and carbon stocks of olive groves on Lesvos were created and values on AGB and carbon stocks were obtained. The results show a necessity for the continuation of field work for further development of methodology for remote AGB estimation. Updated results can be used by policymakers for science-based decision-making in developing a more sustainable agriculture system aimed to store more carbon in agricultural groves at the local and regional levels.

Keywords: remote sensing, GIS, biomass estimation, carbon stocks, olive groves, ecosystem services, agricultural monitoring, spatial modelling

Acknowledgements

I would like to express my profound gratitude to professor Themistoklis Kontos from the Department of Environment of the University of the Aegean. He guided me through GIS, Remote Sensing, and programming technologies and tools and spent long hours explaining and showing me advanced implications for better expressing scientific concepts and ideas.

I am grateful to professor Nikolaos Fyllas and all Fyllas' Research Group from the Department of Environment of the University of the Aegean for letting me join their field trips on Lesvos and guiding me with field research methods.

I would like to thank professor Viktor Lagutov and PhD student Anastasia Kvasha from the Department of Environmental Sciences and Policy of Central European University who patiently and in detail taught me the basics of GIS, Remote Sensing, and modelling, and helped me to better elaborate, express, and visualize my research ideas.

I am extremely grateful to professor Laszlo Pinter for promoting the importance of marathoner stamina in academic life, optimism, and unshakable belief in yourself, and professor Aleh Cherp for giving the understanding of changing life circumstances possibility by following your own agenda.

Furthermore, I would like to thank professor Brandon Anthony for teaching solid quantitative methods and professor Iosif Botetzagias for the intense and useful training in statistical analysis. I am grateful to the Department of Network and Data Science of Central European University for the “Introduction to Programming in Python” course and the “Netology” educational team for the “Advanced Python Development” online course.

Finally, this work would not have been possible without the endless support of my family, extended family, and my fellow classmates from the MESPOM programme who helped me with all challenges of academic life during the global COVID-19 pandemic and encouraged me throughout the work on the thesis.

List of Figures

List of Tables

List of Abbreviations

AGB	Aboveground Biomass
AGCI	Aboveground Carbon Indicator
CAP	Common Agricultural Policy
DBH	Diameter at Breast Height
EC	European Commission
ES	Ecosystem Services
EVI	Enhanced Vegetation Index
GEDI	Global Ecosystem Dynamics Investigation
GNDVI	Green Normalized Difference Vegetation Index
IDW	Inverse Distance Weighting
IPCC	Intergovernmental Panel on Climate Change
IRVI	Inverse Ratio Vegetation Index
LAI	Leaf Area Index
LiDAR	Laser imaging, Detection, and Ranging
NASA	National Aeronautics and Space Administration
NDC	Nationally Determined Contributions
NDVI	Normalized Difference Vegetation Index
NIR	Near Infrared
PAI	Plant Area Index
RS	Remote Sensing
RVI	Ratio Vegetation Index
SAVI	Soil Adjusted Vegetation Index
SR	Simple Ratio
SWIR	Short-wave Infrared
TIRS	Thermal Infrared
TVI	Transformed Vegetation Index
UNFCCC	United Nations Framework Convention on Climate Change
VI	Vegetation Indices

1. Introduction

1.1 General Introduction

Accessing and mapping aboveground biomass (AGB) is crucial for understanding the global carbon cycle. Agricultural lands are providing carbon storage as an additional ecosystem service (ES). Remotely sensed (RS) data can be used to estimate and monitor carbon stored in agricultural groves.

The current thesis presents the testing of a multi-step methodological approach that integrates RS and field data to estimate olive groves (*Olea europaea* L.) on Lesvos Island, Greece. Fusion of satellite imagery (Landsat 8), Laser imaging, Detection, and Ranging (LiDAR) data (NASA's GEDI mission), and field observation may predict AGB and improve estimation and mapping carbon stocks of olive groves on the island of Lesvos, Greece.

Retrieving parameters connected to biomass such as Leaf and Plant Area index (LAI and PAI) from field measurements and GEDI data, the correlation and regression analysis between satellite imagery information on bands and vegetation indices (VI) will be conducted. The possibility of fusing field measurements, GEDI data, and spectral information from Satellites for accessing and mapping carbon stocks of olive groves on the local lever will be investigated.

Developing a methodology for biomass estimation can provide illuminating information for policy-making and sustainable development of agricultural lands.

1.2 Table of Contents

2. Literature Review

2.1 Background and Significance

2.1.1 Climate Crisis Overview

Global COVID-19 pandemic for some time overshadowed the agenda of the world climate crisis, a problem common to all mankind that has not disappeared with the advent of the virus. Human-related factors such as fossil fuel combustion, deforestation, urbanization, and extensive agriculture are responsible for the increase of CO2 concentration in the atmosphere which is responsible for the global temperature rising by 1°C since pre-industrial times (IPCC 2015). To achieve the goal of the Paris Agreement, staying below 1.5°C, global CO2 emissions should be decreased to net-zero by 2050 (IPCC 2018).

At the end of February 2021, the United Nations Framework Convention on Climate Change (UNFCCC 2021) published a report on Nationally Determined Contributions (NDCs) under the Paris Agreement. According to the report, with the national climate action plans developed by 75 nations, countries will be able to reduce greenhouse gas emissions by only 1% by 2030, while the declared figure is 45%.

Reaching this ambitious and not yet seemingly achievable goal is not possible without countries' efforts to change industries systematically and prepare and implement strategies to decarbonize economies. The NDC Global Outlook Report 2019, prepared by the United Nations Development Programme (UNDP) and UNFCCC, developed nations focus on longer-term strategies (LTS), carbon neutrality goals (UNDP 2019).

2.1.2 Ecosystem Services

Maximising carbon storage in the biosphere is one of the objectives of climate change mitigation. Carbon storage is one of many ecosystem services (ES) are offered to mankind by nature for free that are often taken for granted and therefore excluded from the modern economic system and defined as non-market resources (Rashid and Seizov 2012). However, they play an important role in resisting the destructive anthropogenic impact on the planet.

The ES framework is a fundamental natural resource management approach that has gained increasing attention from the scientific community and policymakers (Tallis *et al.* 2008). Researchers assume the framework to be a major future influence for shaping existing environmental policies in the coming decades (Matzdorf and Meyer 2014).

The Millennium Ecosystem Assessment aimed to analyse the anthropological impact on ecosystems recognise four categories of ES: provisioning, regulating, cultural, and supporting services. Provisioning services include products taken from ecosystems, such as food, water, fuel, fiber, biochemicals, and genetic resources. Regulating services benefit from the regulation of ecosystem processes, such as climate, disease, and water regulation, water purification, and pollination. Cultural services include nonmaterial benefits, such as recreation and tourism, aesthetic, inspirational, educational, spiritual benefits, and cultural heritage. Supporting services are necessary for the production of all other ES, such as soil formation, nutrient cycling, and primary production (Alcamo *et al.* 2005).

In case of affecting air quality, ecosystems both bring chemicals into the atmosphere and remove them from it. Climate regulation is a regulating service as well since on the global scale, ecosystems play an important role in climate by sequestering and emitting greenhouse gases.

Carbon sinks are part of ES. They take CO2 from the atmosphere to sustain their life, by which they regulate carbon concentration and mitigate the effects of climate change.

According to the Paris Agreement, "Parties should take action to conserve and enhance, as appropriate, sinks and reservoirs of the greenhouse gases" (UNFCCC 2015). The Intergovernmental Panel on Climate Change (IPCC) claims that the global mitigation goal cannot be met without a significant contribution from carbon storage in ecosystems (IPCC 2019). Nowadays carbon accounting is included in Land Use Land Use Change and Forestry (LULUCF) activities under the Kyoto Protocol, but it does not clarify the carbon stocks in ecosystems, their distribution, quality of the reservoirs, and therefore actions that can affect them positively or negatively (Keith *et al.* 2019).

2.1.3 Agriculture and the Carbon Cycle

Agriculture is responsible for 10% of 2019 world's greenhouse gas emissions, the majority of which are coming from livestock, agricultural soils, and rice production (EPA 2020). Along with it, agricultural lands play an important role in atmospheric CO2 storage globally. They are one of the sources of carbon storage in the terrestrial ecosystem and constitute around 20% of all living terrestrial biomass (Li *et al.* 2015).

The multifunctionality of agricultural systems from the perspective of ES has been increasingly gaining significance and has become one of the main objectives in the design of policies (Fernández-Habas *et al.* 2018). Agricultural lands used for vegetation planting can be classified into several categories of ES. For example, olive groves can provide both provisioning services, such as food (olives and olive oil), and regulating services, such as air quality maintenance and climate regulation. Experts value the provisioning of regulating services (41%) of olive groves more than socio-cultural (30%) and provisioning services (29%), with the "food quality" and "biodiversity conservation" as services with the highest relative weight (Fernández-Habas *et al.* 2018).

While agriculture is considered a huge part of the climate change issue, the potential of olive groves for sequestering carbon in soil and woody compartments and climate change mitigation is widely acknowledged (Michalopoulos *et al.* 2020). The carbon storage capacity of agricultural lands is dependent on climatic conditions, soil properties, and agricultural practices used, such as the tillage practices, types of fertilizer used, and crop regimes, among other factors (Beaufoy 2001; Srivastava *et al.* 2012; Nair *et al.* 2015). Reducing the loss in agriculture and applying management techniques aimed at storing carbon can preserve current terrestrial carbon sink strength and even enhance it (Janssens 2003).

2.1.4 Olive Cultivation on Lesvos

Throughout the Mediterranean region, olive groves are culturally, aesthetically, and ecologically valuable (Moreira *et al.* 2019). They have been cultivated for over 4,000 years, so olive groves have become a crucial part of both the Mediterranean landscape and culture. They are one of the most important and extensively cultivated crops in the region, covering an area of 9.4 million hectares (Ladisa *et al.* 2012; Castro *et al.* 2008).

The olive tree (*Olea europaea* L.) is a typical Mediterranean sclerophyllous species highly tolerant to drought and water shortages (Sofo *et al.* 2004). Apart from being commercially and culturally important, olive is a dominant species in the Mediterranean natural plant community (Höhnel 2019), with the floral composition of olive agroecosystems having been found to be exceptionally close to natural Mediterranean ecosystems. Traditionally, olive groves comprise a mosaic of semi-natural and cultivated areas, including ecological features such as meadows, hedges, and marginal shrublands.

The biodiversity index values of the ecological features which exist in olive groves are consistent with the index values of those ecological components in large areas (Tartaglini *et al.*

2012), implying that olive agroecosystems maintain the ecological composition of the natural landscape features. Olive agroecosystems are therefore considered relatively ecologically stable compared to other agroecosystems, with olive groves providing a sanctuary for many plant and animal species (Loumou and Giourga 2003). The literature reports large numbers of vascular plants, insects, and birds associated with olive grove agroecosystems, and claims that herbaceous diversity in the majority of olive groves exists at the optimal level (Tartaglini *et al.* 2012; Loumou and Giourga 2003). They furthermore provide vital refuges for birds migrating to Northern Europe (Loumou and Giourga 2003).

Olive oil transformed from the Mediterranean to a global product and a multi-billion-euro market (Dios-Palomares and Martínez-Paz 2011; International Olive Council 2015; Scheidel and Krausmann 2011). It has come with a similar transformation of olive groves from traditional to super-intensive, characterised by high use of fertilizers, pesticides, and densely planted olive groves, collectively leading to an array of negative environmental (Neves and Pires 2018), social and economic (Zagaria *et al.* 2017) impacts.

Olive cultivation is one of the most significant agricultural activities in Greece, from economical, social, and ecological points of view (Michalopoulos *et al.* 2020). In 2018-2019, Greek olive oil production amounted to 185 million tonnes, while Spain and Italy – the main other producers of olive oil in the world – were responsible for 1790 and 173.6 million tonnes of olive oil, respectively (EC 2020).

The Greek island of Lesvos located in Eastern Greece is also known as "Olive Island" due to the abundance of olive groves which occupy 28% of Lesvos' surface area (Giourga *et al.* 2008). The olive industry is the third-largest economic activity on Lesvos, after tourism and ouzo production (Kizos and Koulouri 2010). Olive products have great economic importance for Lesvos (Hellenic Agricultural Enterprises 2020; Russo *et al.* 2016). It is the third largest producer in the country, which is, at the same time, the third largest producer in the world.

Olive cultivation for oil production has mostly traditional practices put in place since the activity is deeply rooted in the population's culture (MESPOM 2020). On Lesvos, olive groves are classified as traditional extensive due to their low density of "old" trees which have an irregular pattern of the plantation, and their low yield, low labor and material inputs and manual harvesting (Giourga *et al.* 2008; Fleskens 2007). The olive groves of Lesvos are small-sized and traditionally labour-intensive; they are found on sloping fields and are characterised by limited use of herbicides, diesel, and electricity (Giourga *et al.* 2008; Kizos and Vakoufaris 2011; Russo *et al.* 2016).

Lesvos has a typical Mediterranean climate, with 19,6°C as the mean annual temperature and 700 mm as the mean annual precipitation for 2019 (MESPOM 2020). The Mediterranean region is characterised by warm and rainy winter, hot dry summer, and frequent and intense precipitation events, particularly in autumn (Morugán-Coronado *et al.* 2020). Situated between the arid North African climate and temperate central Europe, the Mediterranean is uniquely positioned and is expected to face relatively high impacts due to climate change (IPCC 2013). In general, the region expects to see increases in temperatures and decreases in precipitation (IPCC 2013). Both temperature and precipitation are drivers of agricultural production, including olive fruit production (Aguilera and Valenzuela 2014).

Olive groves on Lesvos are characterised by relatively low soil fertility as compared to other Mediterranean land-use types, and browsing pressure appears to further diminish the understorey of herbaceous plants associated with the olive groves (MESPOM 2020). However, the analysis based on data provided by the Biodiversity Conservation Laboratory of the Environment Department of the University of Aegean reveals a higher species richness in olive groves on Lesvos than in forest systems (MESPOM 2020).

During the season 2019-2020, 57.600 tons of olives were processed in total on Lesvos, which translates into 13.200 tons of olive oil, with an average production of 230 kg of oil per

ton of olive processed. Out of this, 36.7% was extra virgin olive oil, 18.8% was virgin olive oil and 44.5% was lampante oil (Department of Agriculture 2020). These large production quantities show the relevance of this activity on Lesvos' economy.

Climate change associated with the increased level of greenhouse gases in the atmosphere can affect olive groves. Research has shown that olive trees may be strongly impacted by climate change, especially in Mediterranean climates (Orlandi *et al.* 2010). Olives trees are particularly well suited to the Mediterranean climate of Lesvos, with its warm and dry summers and wet and mild winters. However, the Mediterranean basin in general is considered to be a climate change hotspot (Giorgi 2006) and is expected to get warmer and drier (Aguilera and Valenzuela, 2014).

There is a negative correlation between climate change and olive yield on Lesvos (Georgopoulou *et al.* 2017; MESPOM 2020). Major factors affecting olive yields are precipitation (Ozdemir 2016) and temperature (Gutierrez *et al.* 2009). According to Lesvos' meteorological data which was collected through ground observation at the Mytilene Airport meteorological station, provided by the Greek National Weather Service, in the past 57 years, the annual precipitation on Lesvos is significantly decreasing and the annual mean temperature has already increased by 1.9°C (MESPOM 2020). Other important factors influencing yield are the previous year's yield (MESPOM, 2020), pests (olive fruit fly), cultivar composition, tree density, training degree of mechanism and chemical input, irrigation, soil water condition, and the harvesting mechanism (FAO 2015). The yield also depends on the tree age and pruning (Vossen 2006).

Weather related data show temperature and precipitation change which have a range of impacts on olive yield, with a general decreasing yield predicted as these factors are amplified over the coming 80 years (MESPOM 2020). In the face of climatic uncertainty, the agroecosystems of Greece, which are some of the oldest in the world, will need to adapt. Some

options include conserving soil water content, improving technology and irrigation, campaigning for carbon neutrality within the olive agri-food chain, and enabling future action through local and regional research (MESPOM 2020). By utilizing both the short- and long-term options available, farmers may be able to reduce the shock of decreasing yields (MESPOM 2020).

The age of olive trees on Lesvos agricultural land can reach up to 400 years, according to local knowledge. Due to the local management strategies, trees are not burned or cut for many years and therefore can accumulate carbon for 300-400 years without releasing it into the atmosphere. One of the largest economic sectors on the island, olive production has been central for the well-being of the island inhabitants, as well as a valuable carbon sink for the world. However, environmental uses of olives such as carbon storage and climate change mitigation are underassessed (Kebede and Soromessa 2018).

2.1.5 Carbon Oriented Management of Olive Groves

While modern conventional agriculture is considered to pose one of the major threats to global biodiversity, organic farming can offer an alternative route for ensuring sustainability through the increasing of biological diversity and maintenance of soil fertility (Solomou and Sfougaris 2011). Proper agricultural techniques and sustainable land management, along with the increase in productivity and soil preservation, can also contribute to the removal of a significant amount of CO2 in the atmosphere (Sofo *et al.* 2004).

However, there is still no consensus on how to manage agriculture in a sustainable manner to reduce CO2 emissions for typical Mediterranean crops (Robertson 2000).

Since olives are widely cultivated in the Mediterranean basin, they can play a fundamental role in reducing the expected impact of climate change (Brilli *et al.* 2018). “Carbon

oriented" management of olive groves can be a promising way to increase the carbon storage in agricultural land (Coderoni *et al.* 2014).

Understanding how different management practices of olive groves in general, for example, relating to tillage, fertilizer usage (inorganic and organic), and cropping systems affect the soil properties of olive groves is extremely important. Specifically, regarding olive groves, the average organic carbon stock in olive groves is comparable to forest soil concentrations, highlighting the importance of Mediterranean olive orchards as carbon reservoirs (Panozzo *et al.* 2019).

Since olive groves have wide implications for atmospheric carbon sequestration, it is obvious that the sustainable management of agricultural systems is important for the mitigation of the anthropogenic influence to local ecosystems through adverse farming practices, as well as to the global climate system. Sustainably managed olive agroecosystems can provide a variety of crucial ES, including the provision of food, firewood, and fodder, regulation of water and nutrient cycling, pollination, safeguarding of soil quality, conserving biodiversity, and preserving aesthetic, cultural, and traditional significance (Loumou and Giourga 2003; Brunori *et al.* 2019; Jiménez-Alfaro *et al.* 2020).

Researchers highlight the importance of Mediterranean olive planting for fixing atmospheric CO2 and argue that training agricultural workers, plant density and the use of sustainable farming practices will also help increase the capacity of the orchard system for carbon storage (Sofo *et al.* 2004). For this, Brockett *et al.* (2019) highlight that an interdisciplinary approach to studying the agricultural environment can help to better understand how land is managed and how it affects the people who use it. This can help to develop policies that can improve the understanding of management changes and the efficiency of farming.

Greek target for 2030 is the decrease of greenhouse gases (GHG) emissions by 14% from the 2005 level. Greek National Energy and Climate plan estimates they may overachieve this target by 9-13 percentage points, which can open the opportunities to transfer emissions allocation to the other EU Member States. However, the plan does not include information on how Greece would achieve its commitment that LULUCF emissions do not exceed removals (EC 2019). The objectives of research and innovation are unclear now for the period after 2020, although Greece has a target for carbon intensity reduction (EC 2019).

Regarding the agricultural management practices, in general, the olive plantations of Greece can be classified as either low-input traditional plantations, with few or no chemical inputs, with high labor requirements; intensified traditional regimes that utilize artificial fertilizers and pesticides, and more intensive soil management; and finally intensive modern plantations managed under a highly mechanized system (Beaufoy 2001). While traditional olive cultivation in Greece saw intercropping of olive with cereal or legumes as silvoarable systems (Papanastasis 2009), industrialisation saw multi-functional olive grove production shift toward non-sustainable paths such as mechanisation and intensification, as well as towards monocultures, in order to maximize yields (Moreira *et al.* 2019; Morugán-Coronado *et al.* 2020).

The European Union attempt to support olive farming is the Common Agricultural Policy (CAP). It is the core of the European farming sector and since its inception in 1962 has increasingly become the engine driving agriculture in the region (MESPOM 2020). It primarily consists of three main pillars: income support for farmers, instruments to deal with difficult market situations, and measures for rural development. However, CAP in its present state isn't doing enough to incentivize farming. A major critique is the unjust distribution of benefits; large farmers receive a disproportionately large share of the benefits, while small farmers largely lose out (MESPOM 2020). While CAP payments do supplement farmers' incomes, they

do not do enough to protect small farmers from shocks, and it is becoming increasingly common for farmers to turn to other economic activities to supplement family incomes (Buckwell *et al.* 2017). Nowadays it became hard to ignore the outflow of farmers from the agricultural sector (MESPOM 2020).

Policies should be implemented to transform olive farming on Lesvos into a more carbon oriented and therefore environmentally and socially sustainable business while at the same time reaffirm the olive sector's place as a crucial component of the island's economy and handle the declining number of farmers.

2.2 Overview of Methods for AGB Estimation

Since carbon stocks have a great scientific and political importance, they should be evaluated to provide data to support regional, national, and international policies. This will help in finding the right mitigation actions and trade-offs between different ES. Assessing and modelling carbon stock and carbon sequestration ES is necessary to make balanced and science-based policy decisions.

The adoption of the United Nations Framework Convention on Climate Change (UNFCCC) Kyoto Protocol, which, among other things, allowed vegetational sinks to be offset carbon emissions, sparked controversy over the adequacy of existing methods for estimating and predicting carbon stocks levels (Rosenqvist *et al.* 2003).

Carbon stocks assessments in the literature on ES have largely focused on AGB estimation (Quijas *et al.* 2018), which is central in quantifying and monitoring the stored carbon amount. AGB estimation has received significant attention recently because the change in AGB is associated with the components of climate change (Poudel and Temesgen 2016). Quantifying the spatial pattern of biomass can provide a general picture of the carbon stocks in the region.

Researchers (Quijas *et al*. 2018) highlight that ES models can be an adequate source of information for policy makers only if they incorporate ecological processes, including the evaluation of ES, for which biomass component should be considered. Biomass models are important tools for quantifying biomass and carbon stock. Numerous AGB models exist, although many of them are showing large and significant prediction errors for AGB (Njana *et al.* 2015).

The mapping of AGB, field observation data are used by researchers, as well as RS data. Traditional field method has greater accuracy, however, it is difficult to cover large areas since field work is time- and money-consuming, labor-intensive, and impractical (Maia Araújo *et al.* 1999). Developing approaches combining ground- and space-based observations can help in more accurate assessment and modelling of biomass and carbon stocks.

RS is becoming more popular for field studies for large regional AGB estimates because it is considered more practical and cost-effective (Silva *et al.* 2021). Nowadays RS data has become the primary source for biomass estimation (Lu 2006). In the Kyoto Protocol, among identified areas where remote sensing (RS) technology could be applied to support the treaty implementation, is "quantification of above-ground vegetation biomass stocks and associated changes therein" (UNFCCC 1998). Strategies for AGB estimation using RS tools can include several steps (Figure 1).

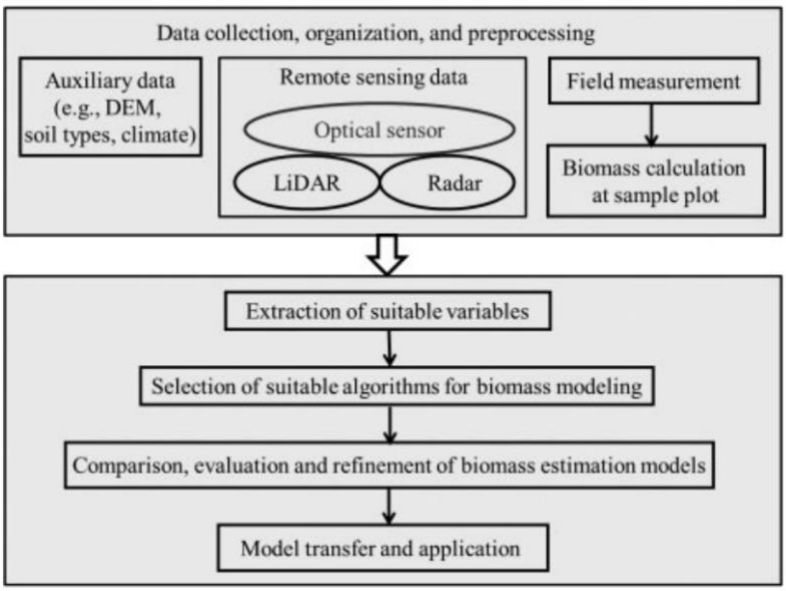

Figure 1. General strategy of biomass estimation modelling using RS techniques (Lu *et al.* 2014).

RS has an advantage in the ability to get information in large areas, including remote regions. AGB can be estimated from different RS sensor types, such as synthetic aperture radars, light detection and ranging (LiDAR), and optical sensors. Radar and LiDAR data have an advantage in their accuracy because they can penetrate the forest canopy and get more information on trunks and branches, which are storing around 60% of the AGB (Bergen and Dobson 1999). Optical sensor data and radar data are suitable for places with a simple tree structure (Lu 2006). Also, the important advantage of RS used to calculate carbon stocks is that it is a systematic observation technique and has historical archives of data, which can be used for the prediction of current and future situations (Rosenqvist *et al.* 2003).

The limitations of these methods are higher costs and big volumes of data to capture (Nguyen and Kappas 2020). Also, even with the development of RS technologies, biomass estimation is still challenging. With an abundance of RS data products, there are no techniques for biomass direct measurement (Nguyen and Kappas 2020).

When RS is combined with field data, the accuracy for the biomass prediction increases (Pandit *et al.* 2018, Rosenqvist *et al.* 2003). The combination of RS and field observations allows to reduce uncertainty and show the spatial distribution of biomass (Du *et al.* 2014).

From the estimation of AGB, aboveground carbon indicator (AGCI) can be obtained. It is expressed in Mg of carbon per km2 and corresponds to the carbon fraction of the oven-dry weight of the woody parts (stem, bark, branches, and twigs) of all living trees, excluding stump and roots (EC 2018). AGCI can be used as an important indicator of monitoring carbon stock change in matters of climate change state monitoring and climate change consequences mitigation.

The AGB needs to be measured and monitored because of its importance to national greenhouse gas inventory and most land-based projects (Ravindranath and Ostwald 2008). Proper assessment and evaluation of AGB are important for sustainable management. Since agricultural practices can be very important in atmospheric CO2 emission and fixation, proper canopy management and agricultural techniques such as, for example, pruning in olive groves could increase the atmospheric CO2 emissions and storage (Sofo *et al.* 2005).

2.2.1 Field Observations

Allometric models are used to access AGB. They are based on correlations between biomass and morphological characteristics such as basal area, height, canopy diameter or volume. In the case of olives, AGB was found strongly correlated with diameter at breast height (DBH) and height; DBH and wood density; and the combination of DBH, height, and wood density (Kebede and Soromessa 2018). Canopy cover and height are linear with DBH and tree height, respectively, and have great potential for forest volume estimation (Chen *et al.* 2021).

"Plot method" is widely used by researchers in agriculture for estimating and monitoring biomass and carbon stock changes. Measurement and estimation of AGB stock can include the following steps (Ravindranath and Ostwald 2008; Woldemariam 2015) (Figure 2).

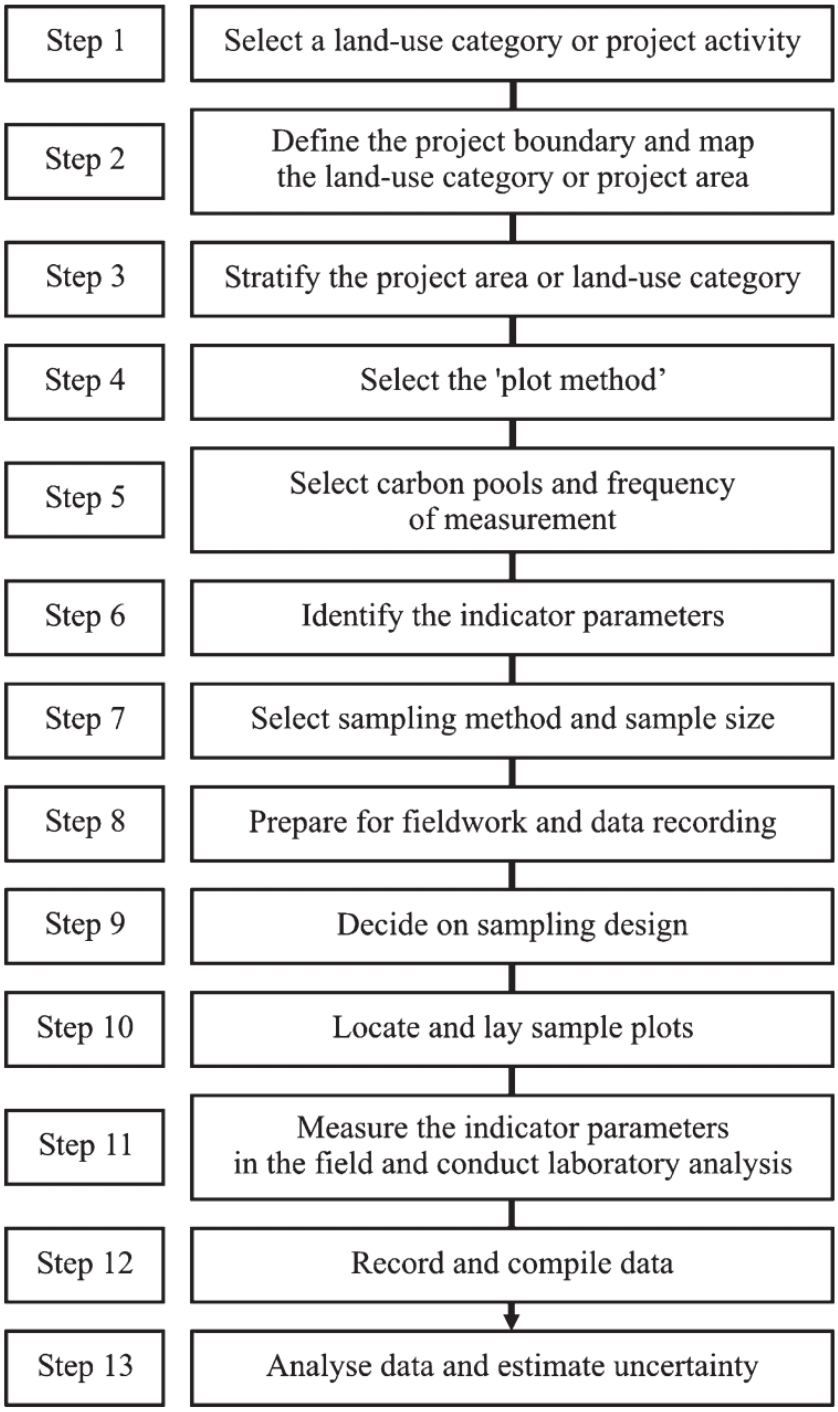

Figure 2. Steps in measurement and estimation of AGB stock (Ravindranath and Ostwald 2008).

For estimating biomass, several parameters can be used. Among the most popular are stand volume, stump diameter, Leaf Area Index (LAI), or Plant Area Index (PAI).

Stand volume is traditionally estimated by measuring canopy height and diameter from harvested trees (Boisvenue *et al.* 2016; Hyyppä *et al.* 2000). Nowadays, combining RS data and field retrieved data has become an efficient methodology to generate full-cover estimations of forest stand volume (Mauya *et al.* 2019; Saarela *et al.* 2015; Santoro *et al.* 2011).

Stump diameter is an important tree variable used to describe stand structure, estimate tree volume, and select inventory sample trees (Corral-Rivas *et al.* 2007).

LAI is a key characteristic that shows exchanges of mass and energy within a vegetated ecosystem. It is one half of the total leaf area per unit ground surface (Chen and Black 1992). It is linked to canopy cover through the gap distribution within the canopy.

PAI is a closely related to LAI indicator which in addition to leaves also includes all canopy structural elements such as branches and trunks. The numeric difference of these indices is small, for instance, in dense broadleaf forests LAI ≈ 93% PAI (Tang *et al.* 2012), and this difference is often neglected (Tang and Armston 2019).

2.2.2 GEDI Data

LiDAR RS is a powerful tool for estimating canopy height and vegetation parameters (Adam *et al.* 2020) and is considered the most advanced technology to assess forest AGB. It is widely used to derive LAI (Jensen *et al.* 2008; Wang and Fang 2020), a parameter that can be used for biomass estimation, and gathering accurate data on the vertical structure of forest.

Many RS products provide data that can be used for collecting data for calculating and mapping AGB. Among a few non-atmospheric space-based LiDAR missions are Shuttle Laser Altimeter (SLA), The Ice, Clouds, and Land Elevation Satellite (ICESat), and ICESat2. The

recent National Aeronautics and Space Administration (NASA) Global Ecosystem Dynamics Investigation (GEDI) project is one of them. It was selected as part of NASA's Earth System Science Pathfinder Earth Ventures 2 competition to fill the gap in global observations of vegetation canopy structure.

GEDI was launched from Cape Canaveral, Florida in the Dragon capsule of SpaceX CRS-16 on board of Falcon 9 rocket and installed on the Japanese Experiment Module-Exposed Facility on board of the International Space Station in December of 2018. Its data products offer three-dimensional forest structure measurements derived from terrestrial laser scanning and airborne discrete return of waveform LiDAR (Tang and Armston 2019).

GEDI gathered information on vegetation over areas between ~52°N and ~52°S, coverage is limited due to the ISS orbit inclination. During its two years mission (2019-2020), it sampled 4% of the planet's surface (Dubayah *et al.* 2020). It consists of two lasers producing eight beams with 25 m footprint resolution on the three-dimensional structure of vegetation and their aboveground carbon content.

Along with other similar products, it is used to produce wall-to-wall AGB maps. It is a geodetic-class laser altimeter and the first space-based LiDAR measuring ecosystem structure (Dubayah *et al.* 2020). GEDI was used in the Mediterranean region for studying pine forests (Guerra-Hernández *et al.* 2020).

For canopy cover and LAI, there are a large number of data sets, such as MODIS and Landsat, however, measurements of vertical canopy structure are not largely available (Tang and Armston 2019). The uniqueness of GEDI is in its ability to specifically retrieve vegetation vertical structure. The main goal of the project is to collect data that allow receiving information on canopy structure, biomass, and carbon stocks.

The products derived from this data contain among others canopy height and LAI. Canopy cover is a biophysical parameter widely used for describing the spatial geometric

properties of vegetation. Canopy cover definitions depend on the measuring techniques, such as whether the measurement is acquired at a specific viewing angle or over the entire hemisphere, and whether a tree crown is considered as an opaque object including gaps within the canopy. The GEDI derived canopy cover is the percent of the ground covered by the vertical projection of leaves, branches, and stems only (Tang and Armston 2019) (Figures 3 and 4).

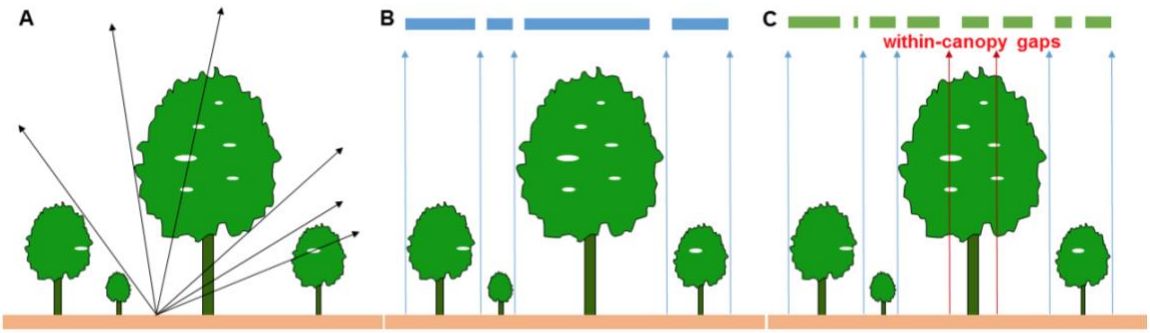

Figure 3. Three types of canopy cover: canopy closure (A), crown cover (B), and canopy fractional cover (C). GEDI will only produce canopy fractional cover (Tang and Armston 2019).

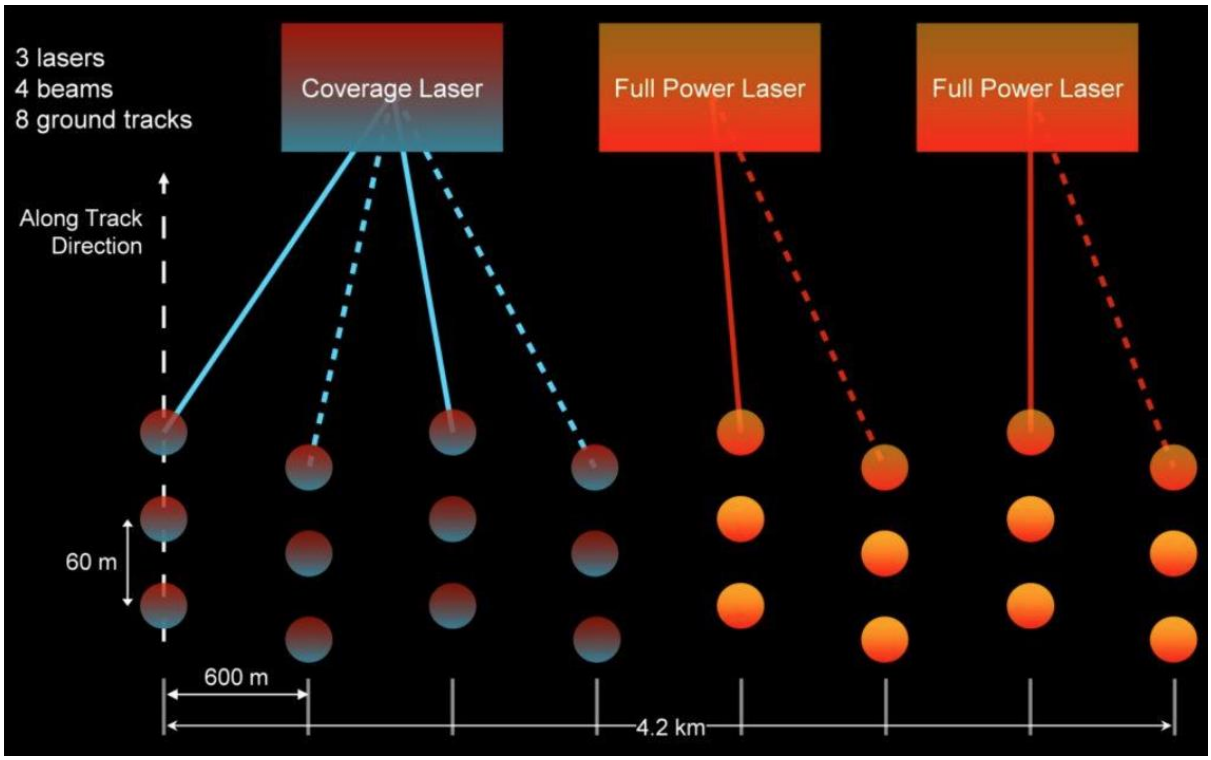

Figure 4. GEDI beam ground-track configuration (Dubayah *et al.* 2020).

One of GEDI data limitations is the lack of representativeness. LiDAR with eight beams at a distance of 600 meters from each other measures the surface at points with a diameter of 25 m at each footprint every 60 m along track, therefore most of the land surface leaves without observations. GEDI is not suitable for targeting rare forest change events such as selective logging, implementation at the local scale, or tracking events through time (Potapov *et al.* 2021).

Vegetation structure is the aboveground spatial distribution of individual tree crowns that is closely linked to ecological functions and services. Its key metrics include total canopy cover and its vertical profile, LAI or PAI, and its vertical profile (Tang and Armston 2019). GEDI's product L2B includes canopy cover, PAI, Plant Area Volume Density, and Foliage Height Diversity.

Vertical LAI which is a vertical variation of the index is closely related to foliage-height profiles. Different LiDAR systems are capable of deriving highly accurate LAI and profile data, however, GEDI's is the only database with the most precise footprint scale of ~25 m (Tang and Armston 2019).

Since LiDAR data is usually spatially discontinuous, biomass prediction can be integrated with radar and passive optical imagery, typically using machine learning algorithms, although obtained data can have poorer resolution and be inaccurate (Gonçalves *et al.* 2017).

2.2.3 Landsat 8 Data

RS data and Landsat 8 Operational Land Imager in particular is an effective and widely used method for AGB estimation (Li *et al.* 2020). Landsat 8 product bands in red, green, blue (RGB), and near-infrared (NIR) wavelength ranges spectrum and RGB VI are used in vegetation biomass estimation models (Poley and McDermid 2020).

According to the United States Geological Survey (USGS), Landsat 8 Band 4 (red) with wavelength 0.64-0.67 is used to discriminates vegetation slopes, Landsat Band 5 (NIR) with wavelength 0.85-0.88 is used to emphasize biomass content and shorelines (USGS 2016).

Red and NIR bands are used for recognising green vegetation, Red for areas where LAI exceeds 2, NIR responds significantly to changes in moderate-to-high vegetation density with LAI from 2 to 6 (Gitelson 2004). Green vegetation exhibits strong absorption in the Red range of the spectrum. In the NIR range, green vegetation strongly reflects incident irradiation (Gitelson 2004).

A plant's greenness can be measured using remote sensing indices that measure its reflectance. These indices can be used to estimate the AGB. Spectral VI were used as indicators of temporal and spatial variations in vegetation structure and density.

To estimate AGB, indices that measure plant greenness based on reflectance in the near-infrared and visible wavelengths are used (Gitelson 2004; Prabhakara *et al.* 2015).

Various VI such the Normalized Difference Vegetation Index (NDVI), the Ratio Vegetation Index (RVI), the Soil Adjusted Vegetation Index (SAVI), the Modified Soil Adjusted Vegetation Index (MSAVI), and Optimized Soil Adjusted Vegetation Index (OSAVI), all derived from red and NIR bands, are linked to green vegetation biomass and LAI (Prabhakara *et al.* 2015). The highest R2 value (0.94) was reported in the research where NDVI and number or other VI such as NGRDI, CVI, GLI, RVI, VARI, and WDRVI were used for modelling maize AGB, along with red and green bands (Han *et al.* 2019).

For monitoring and mapping variation in vegetation cover in Greece, Enhanced Vegetation Index (EVI) and LAI are used for forest cover assessment in Crete island (Elhag *et al.* 2021), as well as the Bare Soil Index (BSI), Tasseled Cap Greenness (TCG), and Tasseled Cap Brightness (TCB) (Polykretis *et al.* 2020), representing soil conditions as well.

NDVI is considered the most popular index connected to biomass estimation, it enables assessment and monitoring of changes in canopy biophysical properties including LAI (Gitelson 2004). For accessing biomass, researchers claim that NDVI could outperform other indices (Poley and McDermid 2020). However, in the case of places with a lower density such as pastures, standard NDVI performed poorly in estimating biomass (R2 = 0.26) and more accurately estimated by VI based on wavelengths located in the red edge. Other indices such as MNDVIs yielded higher correlations with biomass (mean R2 = 0.77 for the highest 20 narrow band NDVIs), while Simple Ratio (SR) yielded the highest correlation coefficients with biomass as compared to narrow band NDVI and the Transformed Vegetation Index (TVI) (average R2 = 0.80, 0.77 and 0.77 for the first 20 ranked SR, NDVI and TVI respectively) (Mutanga and Skidmore 2004).

Apart from NDVI, the most commonly used indices are Green Normalized Difference Vegetation Index (GNDVI) and OSAVI, GRVI/NGRDI, ExG, GLA/GLI/VDVI, VARI. They are also the most commonly used in vegetation biomass estimation models (Poley and McDermid 2020).

TVI was most accurate in estimating high ranges of biomass (R2 = 0.86), while the NDVI was less accurate in estimating low and medium biomass ranges (Prabhakara *et al.* 2015).

The variables that best predicted AGB, in order of importance, were the bands that belong to the region of red and near and middle infrared (López-Serrano *et al.* 2019). Also, among predictor variables for biomass estimation models are red and NIR bands, slope (β), Wetness Index (WI), NDVI, and MSAVI2 (López-Serrano *et al.* 2016).

In the case of quantifying the density of vegetation ground cover in olive groves in the Mediterranean, Inverse Ratio Vegetation Index (IRVI) was found to be the most sensitive index accounting for 82% ($p < .001$) of the variability of VGC density. RVI most accurately distinguished VGC densities > 80% in a cover interval range of 10% ($p < .001$), while IRVI

was most accurate for VGC densities < 30% in a cover interval range of 15% ($p < .01$). IRVI, NRVI, NDVI, GNDVI, and SAVI differentiated the complete series of VGC densities when the cover interval range was 30% ($p < .001$ and $p < .05$) (Lima-Cueto *et al.* 2019).

2.3 Research Gap

One of the reasons for having difficulties associated with linking assessment of ES to decision-making is the lack of data required to develop an assessment at a local level (Fernández-Habas *et al.* 2018). The service of carbon storage of olive groves AGB is underrepresented in the research literature and policy documents.

Optical sensor data products, especially Landsat, are widely used for biomass estimation. However, they are not suitable for vertical vegetation structure such as canopy height, only for the development of horizontal vegetation structure such as the canopy cover (Hudak *et al.* 2002). The use of the stereo-viewing capability of various optical sensor data can provide a better representation of the vertical structure. The integration of vertical structure features and optical spectral response and textures in a biomass estimation model may be a new direction to improve the biomass estimation accuracy but has not been paid enough attention (Lu *et al.* 2014).

Few studies tested the use of LiDAR to estimate AGB linking ground measurements up to satellite observations (Puletti *et al.* 2020). To fill this gap, we performed a study on olive groves on Lesvos where field inventory, Landsat satellite images, and the recent spaceborne GEDI data were simultaneously acquired.

2.4 Aim and Objectives

Researchers use and develop different approaches and methods to assess AGB, based on both field and remote sensing observations. The aim of the study is to examine the ability of LiDAR data and satellite imagery to estimate AGB and carbon stocks of olive groves on Lesvos Island, Greece.

In order to achieve the aim of the research, the objectives of this study are:

1) to use GEDI for estimating and mapping AGB and carbon stocks of olive groves at the local level;
2) to examine the potential of fusing satellite spectral information and vegetation indices with GEDI and field observation for calculating AGB and carbon stocks.

As a physical location for the development of the method, the case of Lesvos Island, Greece, was used, where it was possible to conduct field work to estimate the biomass of *Olea europaea* L. groves.

3. Materials and Methods

The common way to estimate biomass from RS data was used. It contains two steps: first, field measurements of AGB are obtained from sample plot data with allometric equations, which allow estimating the tree-level biomass from different parameters, for example, diameter, height, and wood density (Chave *et al.* 2005, 2014). Second, the field measurements are related to the same places to RS data on the structure, such as canopy height, and then applied together to predict biomass in the hardly accessible locations (Asner and Mascaro 2014; Drake *et al.* 2003; Treuhaft *et al.* 2010).

3.1. Study Area

The study area was the island of Lesvos, Greece. For this area, Satellite and RS data were retrieved. Field work was carried out there on olive (*Olea europaea* L.) groves. Field work was conducted to evaluate total vegetation biomass and calculate LAI. Field surveys were conducted in February-May 2021.

3.2. GEDI L2B Product

LiDAR data from GEDI L2B standard data product was used for retrieving Plant Area Index (PAI) (Dubayah *et al.* 2020). The purpose of the L2B dataset is to extract biophysical metrics from each GEDI waveform. These metrics are based on the directional gap probability profile derived from the L1B waveform and include canopy cover, PAI, plant area volume density, and foliage height diversity. For each laser footprint, it contains latitude, longitude, elevation, vegetation height, cover, PAI, and also vertical profile metrics for cover and PAI.

GEDI data was used for retrieving data as well on the height of trees range (with 5 m step) and accurate height of trees (Appendix I).

For simulated AGB estimates for GEDI data, algorithm flow for obtaining AGB values from LAI described below was used. It was developed by Fyllas' Research Group during field work.

3.3. Landsat 8 Bands and VI

Landsat 8 Satellite Images were downloaded from the USGS Earth Explorer data portal (USGS 2021) specifically for GEDI points dates and dates of field work within a time window of 15-20 days. Based on the literature review, 7 following VI were chosen (Table 1). Data for all bands (Band 1 – Coastal aerosol; Band 2 – Blue; Band 3 – Green; Band 4 – Red; Band 5 – NIR; Band 6 – SWIR 1; Band 7 – SWIR 2; Band 10 – TIRS) was retrieved and selected VI were calculated from it using Python (Appendix IV).

Table 1. Landsat 8 derived VI and their formulas.

VI	Formula
NDVI	(NIR − R) / (NIR + R)
IRVI	R / NIR
RVI or SR	NIR / R
GNDVI	(NIR − G) / (NIR + G)
SAVI	(NIR - R) / (NIR + R + 0.5)) * (1 + 0.5)
TVI	√(NDVI)+0,5
EVI	2.5 * ((NIR - R) / (NIR + 6 * R – 7.5 * B + 1))

3.4. Sampling Algorithm

The algorithm for selecting random points from GEDI data was developed in order to conduct field observations on selected plots. For this, GIS software ArcMap 10.2.2 (ESRI 2014) and Python 3.7 programming language (Pilgrim and Willison 2009) were used.

Olive grove areas were classified into 12 categories in terms of geology, slope, and elevation. All geology types on the island have been divided into 3 categories based on the amount of nutrients the soil can supply to plants. Slope was categorized into 2 classes, up to 7% and more than 7%. Elevation was categorized into 2 classes, up to 200 m and more than 200 m. In each of 12 categories 10 plots were randomly selected. Since no points existed for the two categories, a total of 108 points were obtained.

The area of Lesvos was divided into three geographical areas (Eastern, Central, Western Lesvos) with borders based mainly on municipalities distribution (Figure 5).

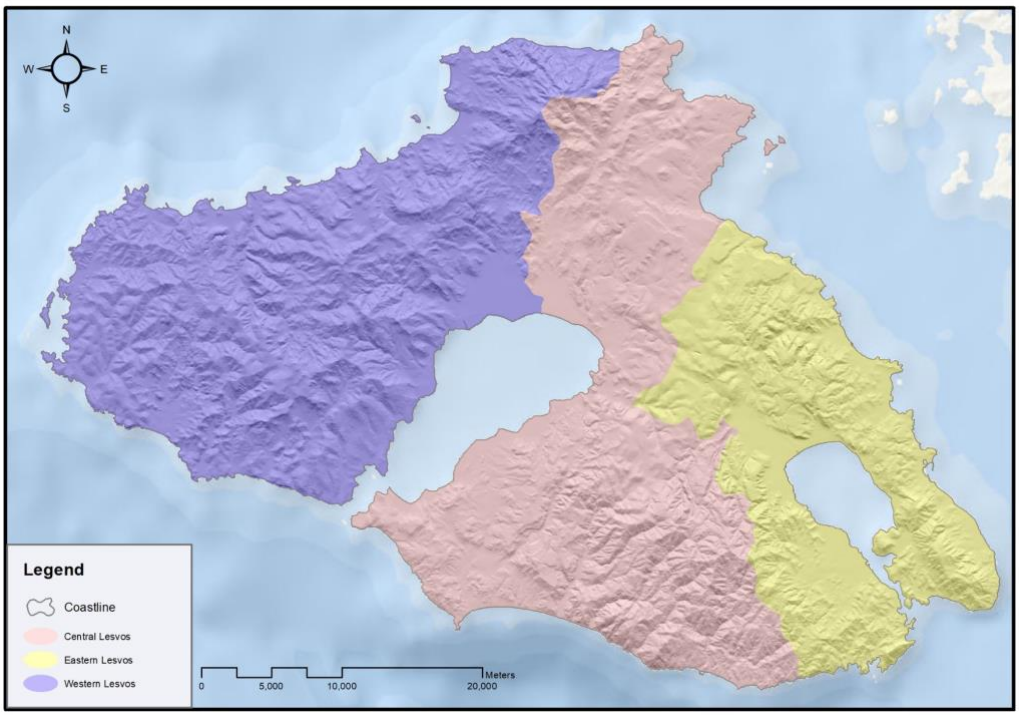

Figure 5. Map of geographical distribution of Lesvos.

Random points were selected based on the percentage of olive groves in each geographical area. Calculations showed that from the whole area of Lesvos olive groves, 40% of groves are located in the Central part, 40% are in the Eastern part, and the rest 20% are in the Western part of the island. Therefore random 10 points for each of 12 categories were distributed accordingly: 4 points for the Eastern part, 4 points for the Central part, and 2 points for the Western part.

Data on olive groves distribution (Figure 6) was retrieved from the Greek Payment Authority of Common Agricultural Policy (OPEKEPE 2021).

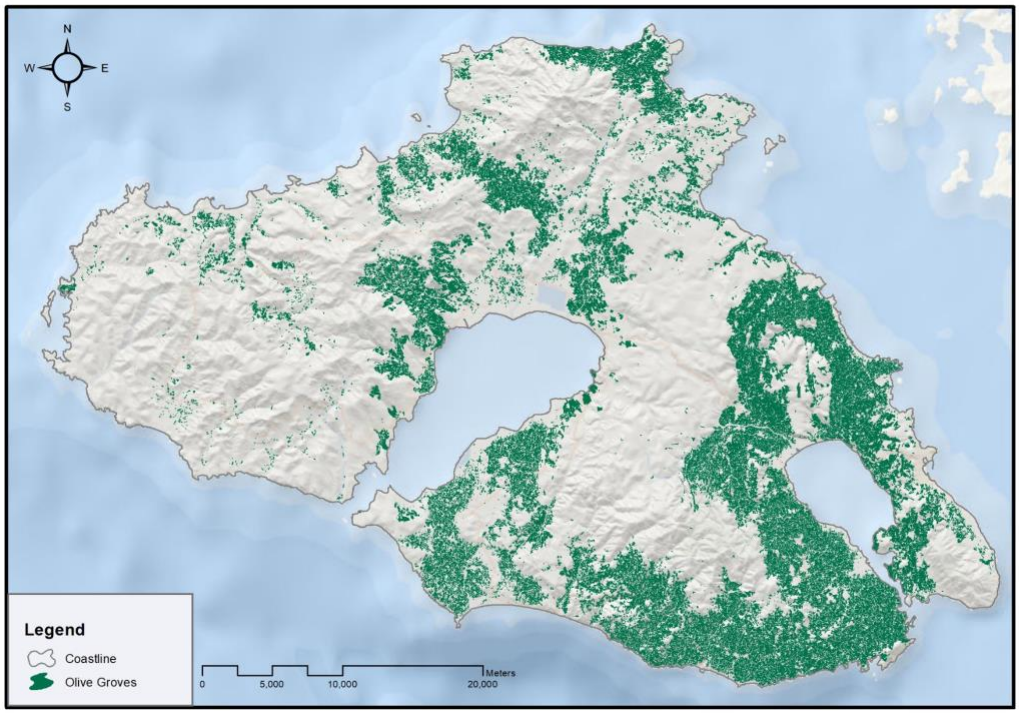

Figure 6. Map of olive groves on Lesvos.

From the digital elevation model of Lesvos, data on elevation and slope for the territory of Lesvos were selected (Figures 7 and 8).

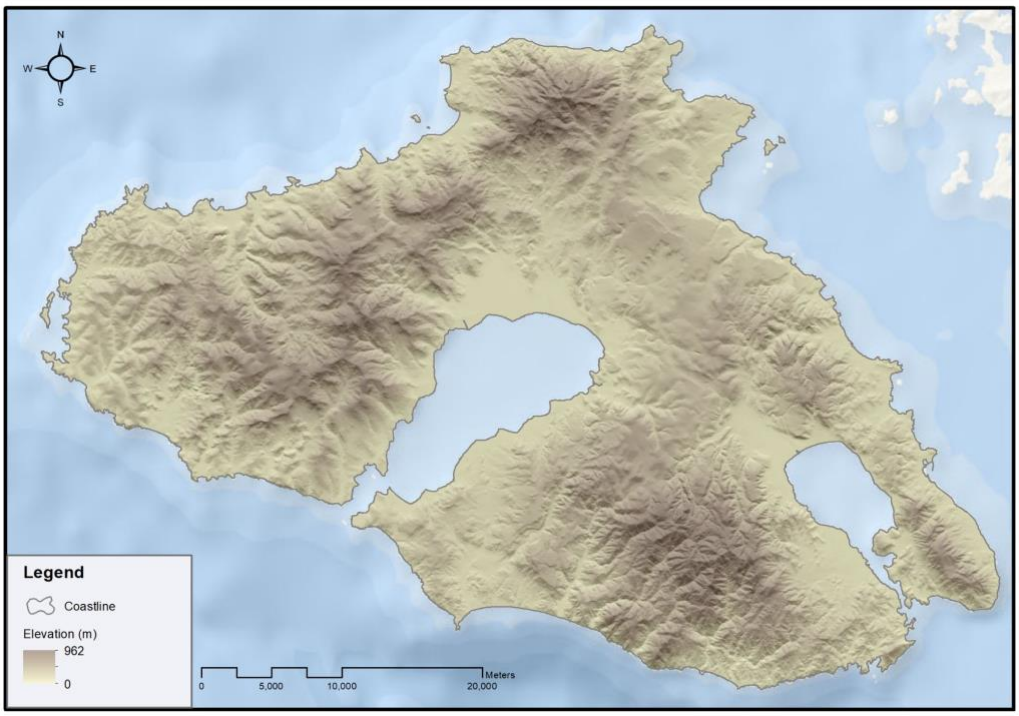

Figure 7. Elevation map of Lesvos.

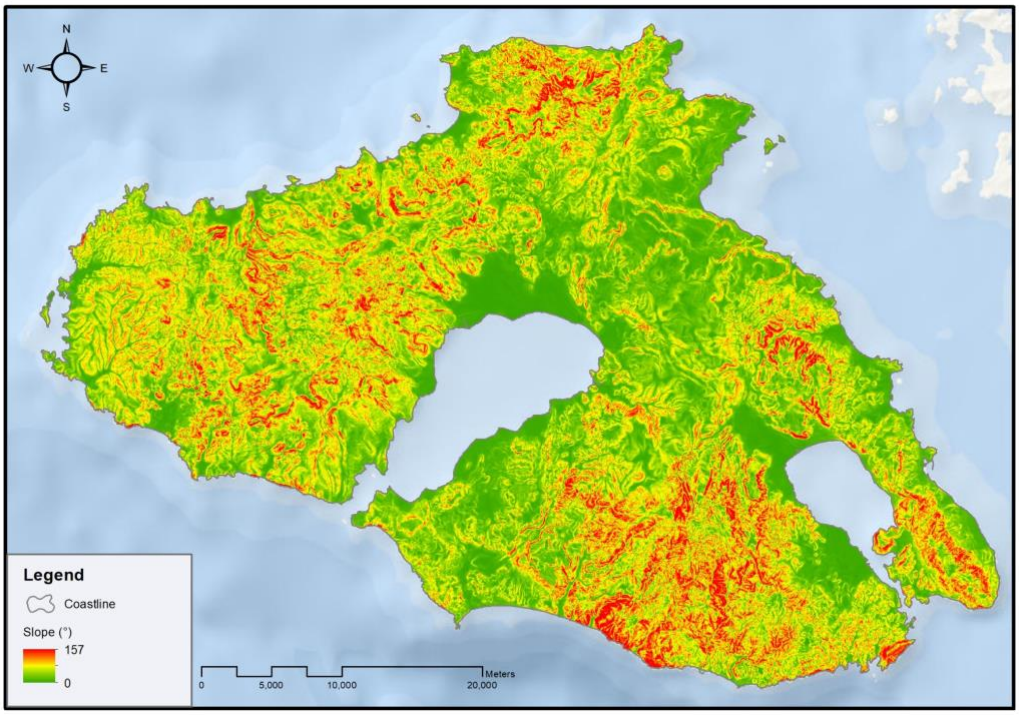

Figure 8. Slope map of Lesvos.

Data on the elevation and the slope was reclassified into 2 categories each (Figures 9 and 10), based on the methodology described above, for future usage in the sampling model.

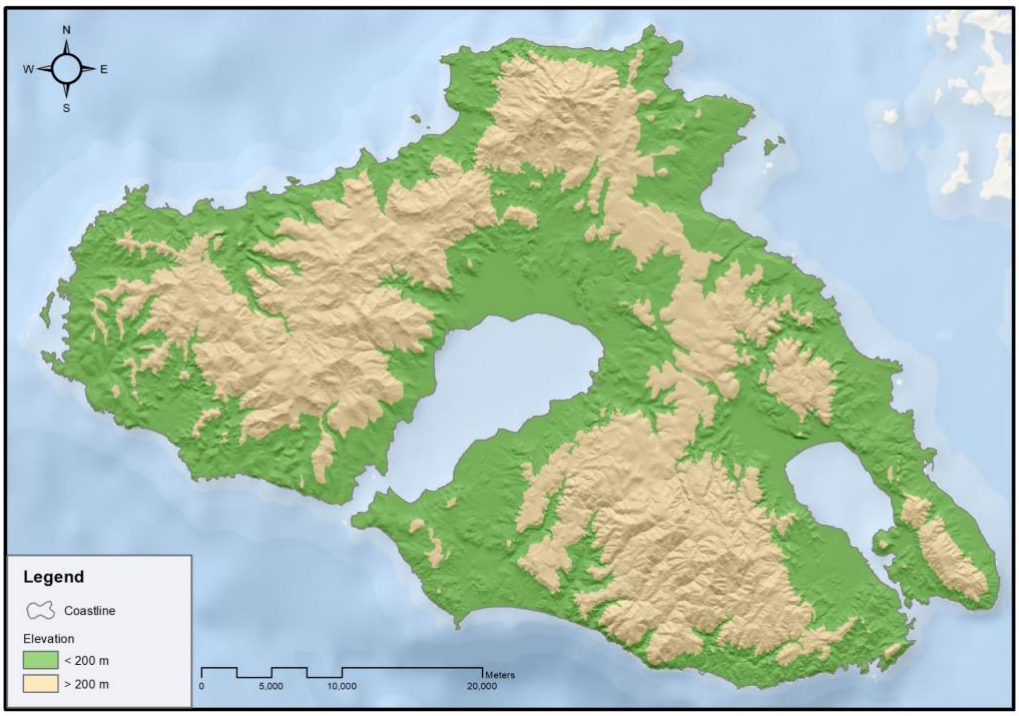

Figure 9. Map on reclassified elevation on Lesvos.

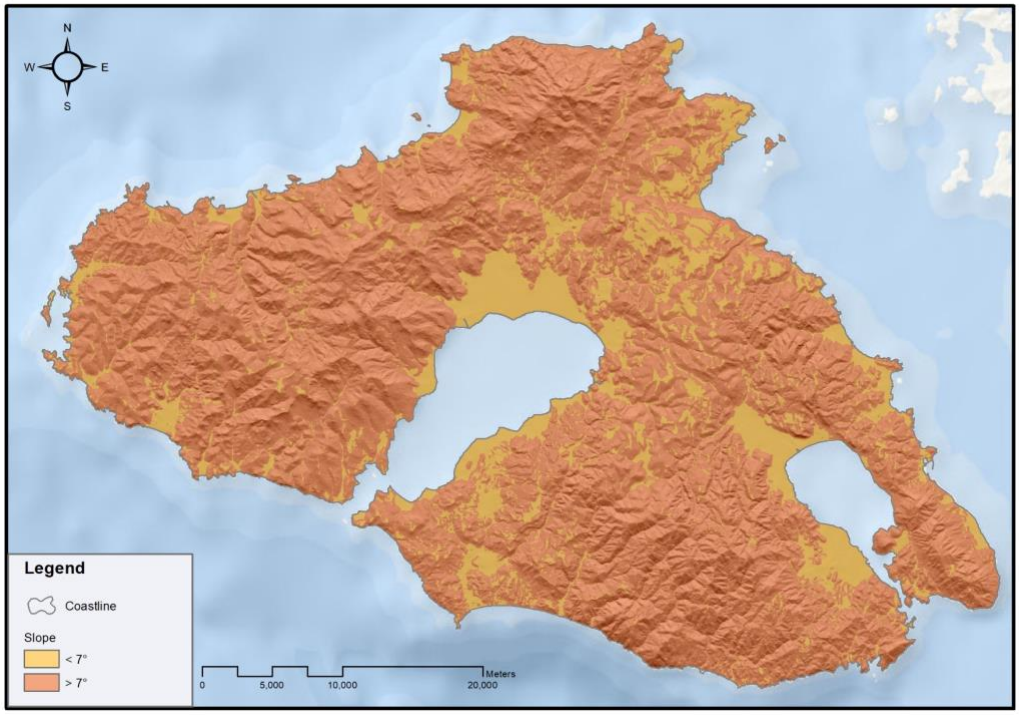

Figure 10. Map of reclassified slope on Lesvos.

The geology of Lesvos was classified into 3 categories based on geology types (Figure 11).

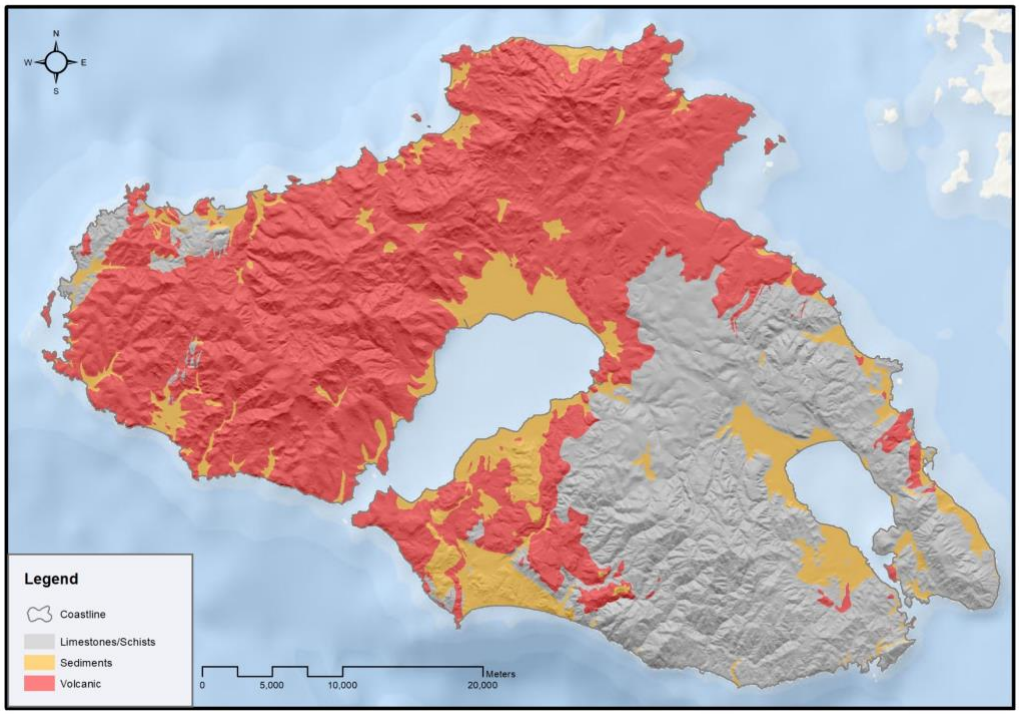

Figure 11. Map of reclassified geology types of Lesvos.

Using Python (Appendix I), data from the GEDI L2B product was retrieved for the specific area of Lesvos for all dates of observation. Quality and Sensitivity flags were checked and taken into consideration and values with no data were removed. For each file, information on date and time, coordinates, elevation, height, canopy cover, and PAI was retrieved, as well as data on the vertical profile of tree heights (Figure 12).

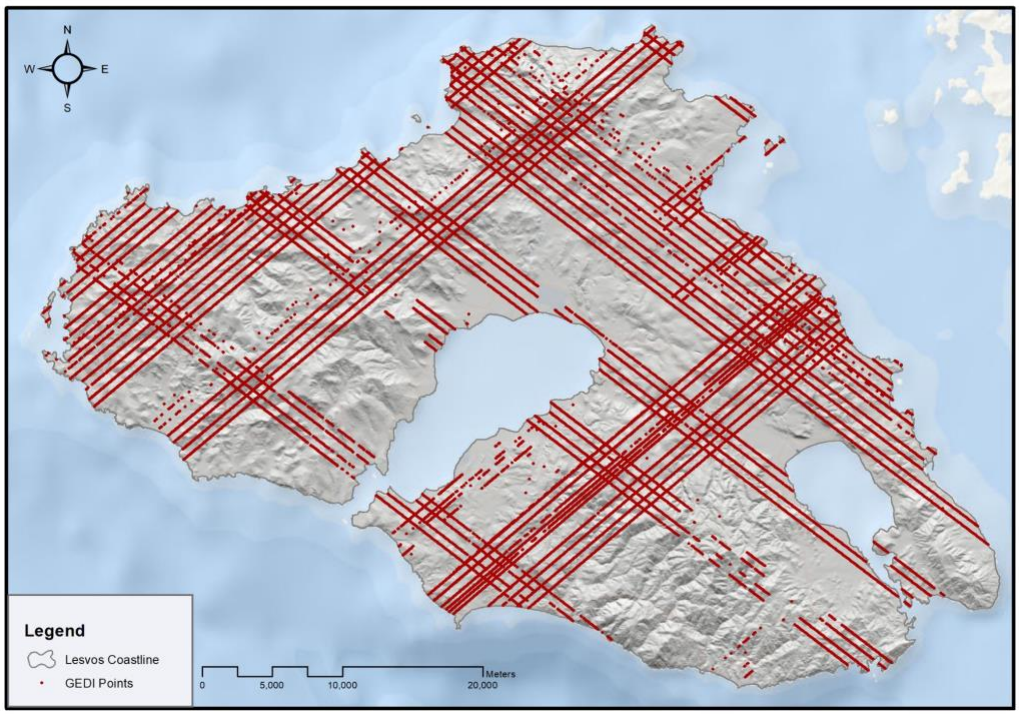

Figure 12. Map on initial GEDI points for Lesvos.

All points were categorized by date (Figure 13).

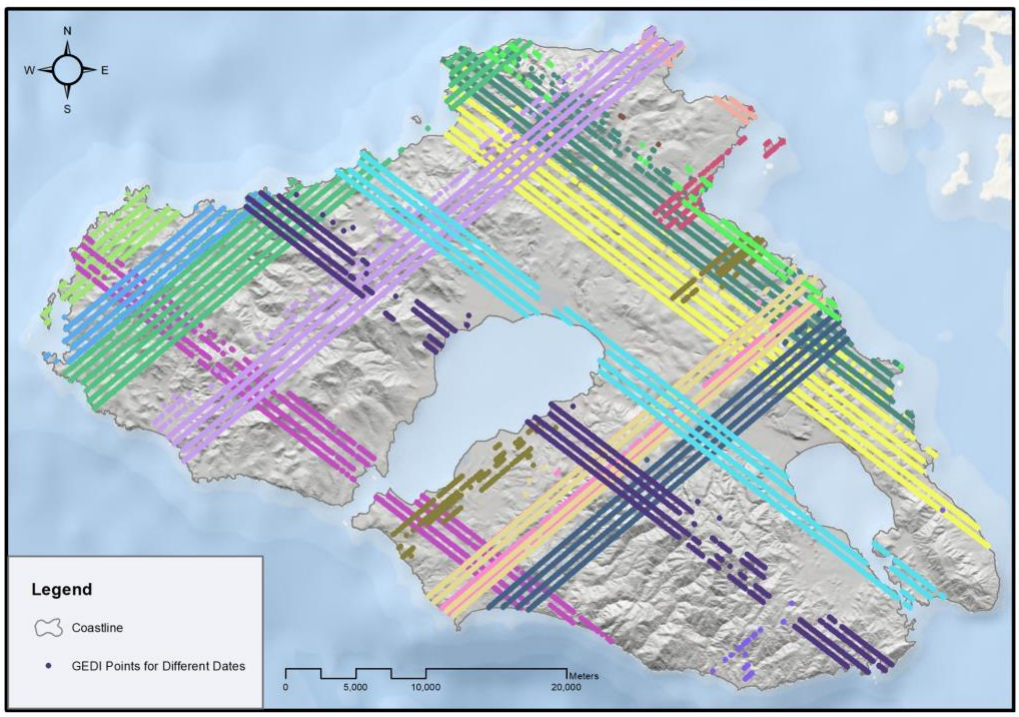

Figure 13. Map of GEDI points categorised by date.

In Python, a fishnet of squares of 100x100 m was created (Appendix II) and masked for Lesvos coordinates (Figure 14).

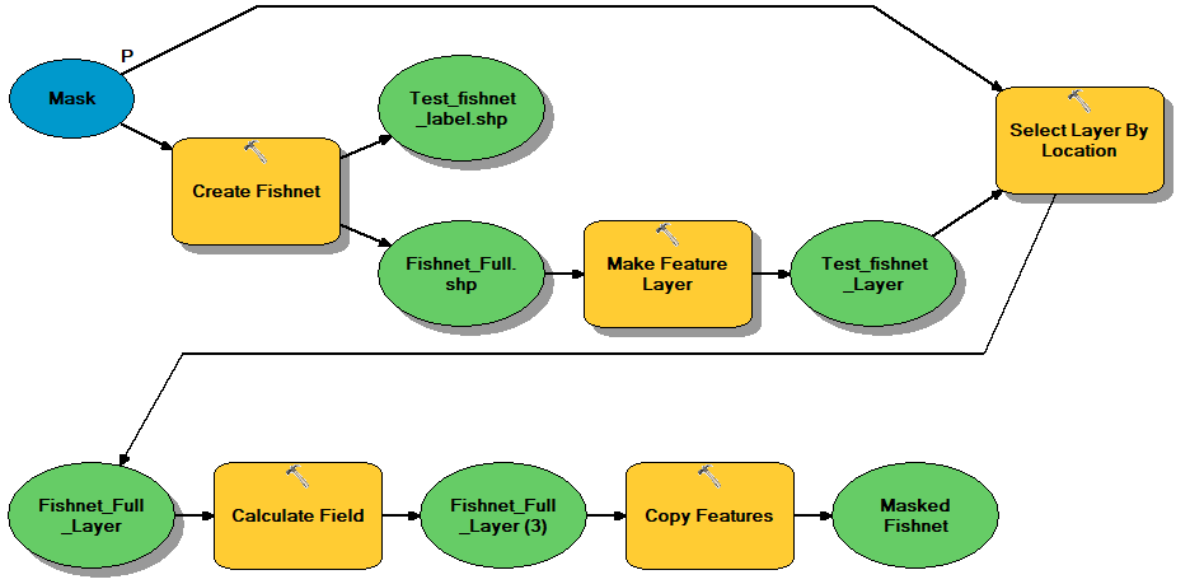

Figure 14. Model for creating the fishnet for Lesvos.

Then, the fishnet was masked for GEDI points falling on olive groves (Figures 15 and 16).

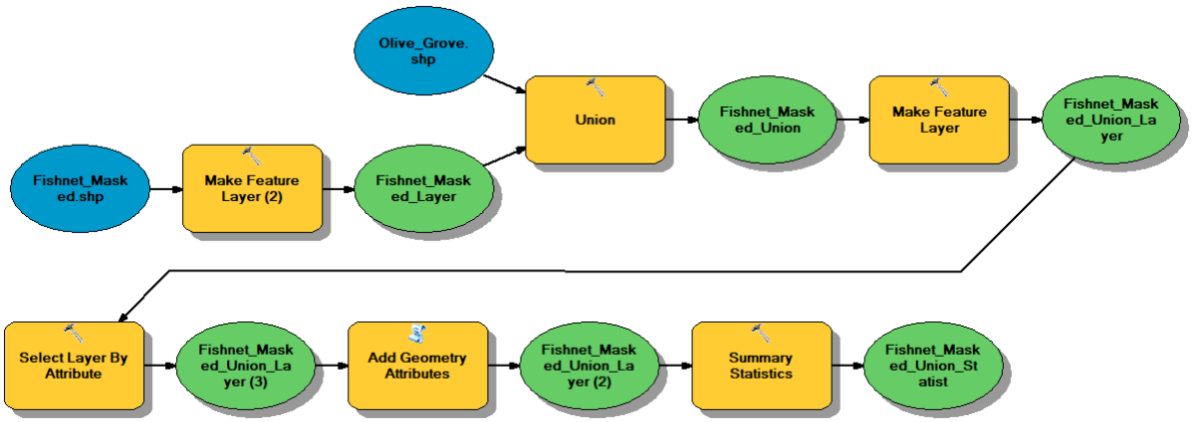

Figure 15. Model for calculating the area of fishnet cells having olive groves for each geographical area.

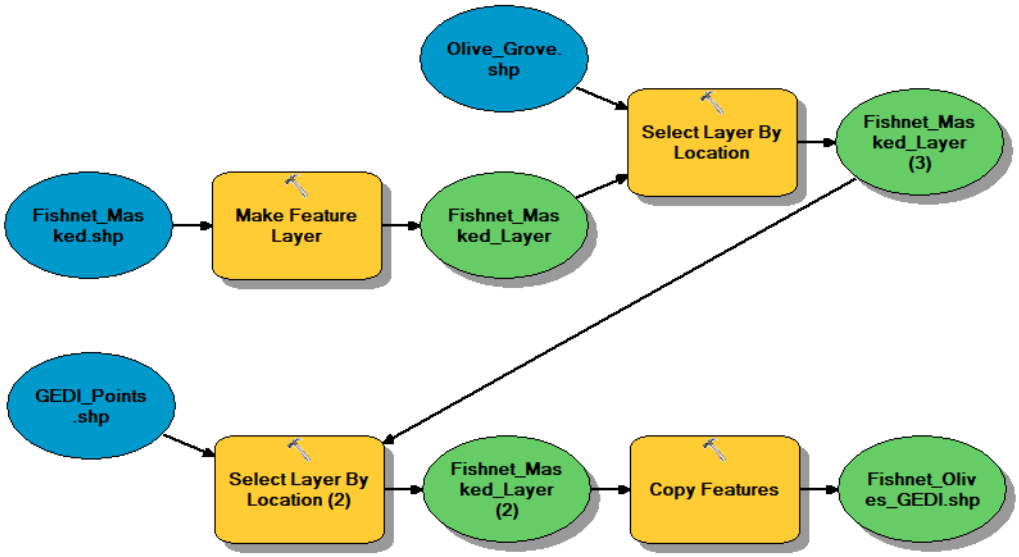

Figure 16. Model for masking the fishnet for GEDI point on olive groves on Lesvos.

Each fishnet's cell was assigned into one of 12 categories based on geographical distribution on Lesvos, geology, slope, and elevation (Figures 17 and 18, categories are described in Table 2).

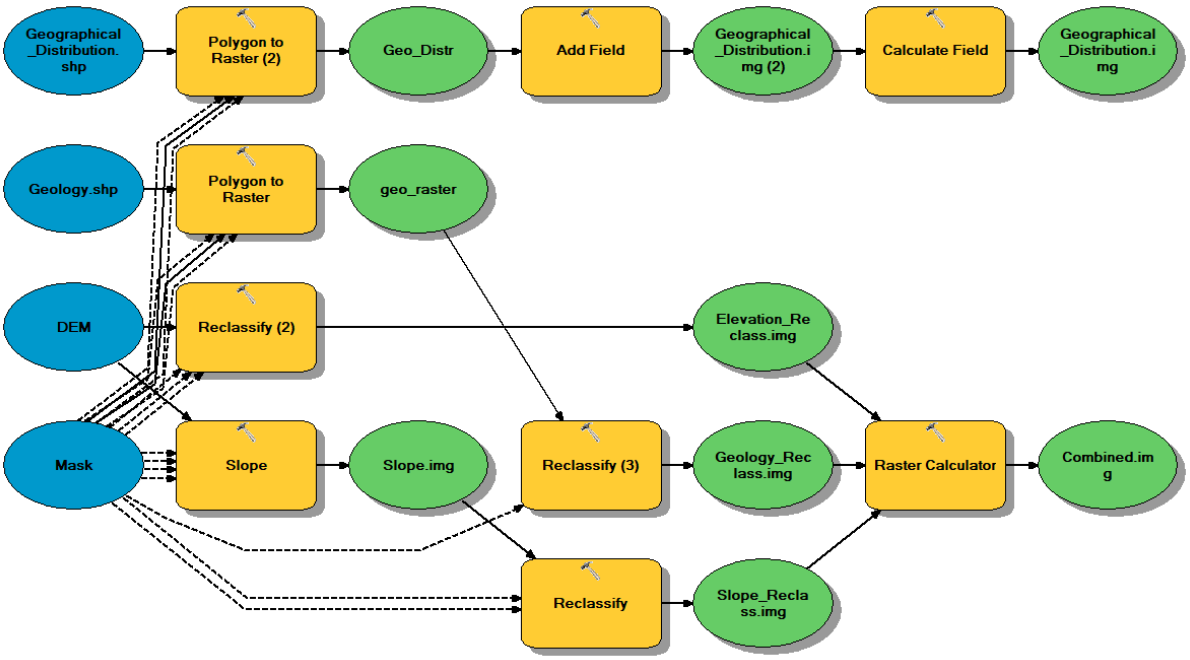

Figure 17. Model for assigning the fishnet cells into 12 categories based on geographical distribution, geology, elevation, and slope.

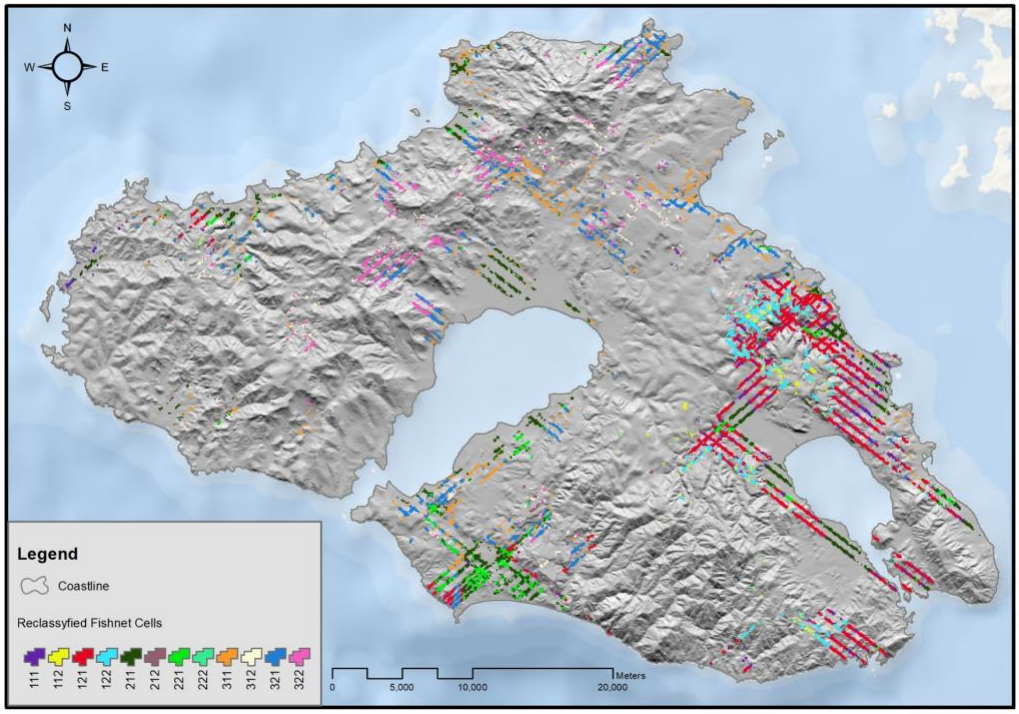

Figure 18. Map of cells on the fishnet created for Lesvos reclassified by geology types, slope, and elevation.

Table 2. Reclassified categories of cells.

Category	Geology Type	Slope	Elevation
111	Limestones/Schists	<7°	<200 m
112	Limestones/Schists	<7°	>200 m
121	Limestones/Schists	>7°	<200 m
122	Limestones/Schists	>7°	>200 m
211	Sediments	<7°	<200 m
212	Sediments	<7°	>200 m
221	Sediments	>7°	<200 m
222	Sediments	>7°	>200 m
311	Volcanic	<7°	<200 m
312	Volcanic	<7°	>200 m
321	Volcanic	>7°	<200 m
322	Volcanic	>7°	>200 m

For each plot, the distance from the center of the fishnet's polygons to the nearest GEDI points falling on olive groves was calculated (Figure 19).

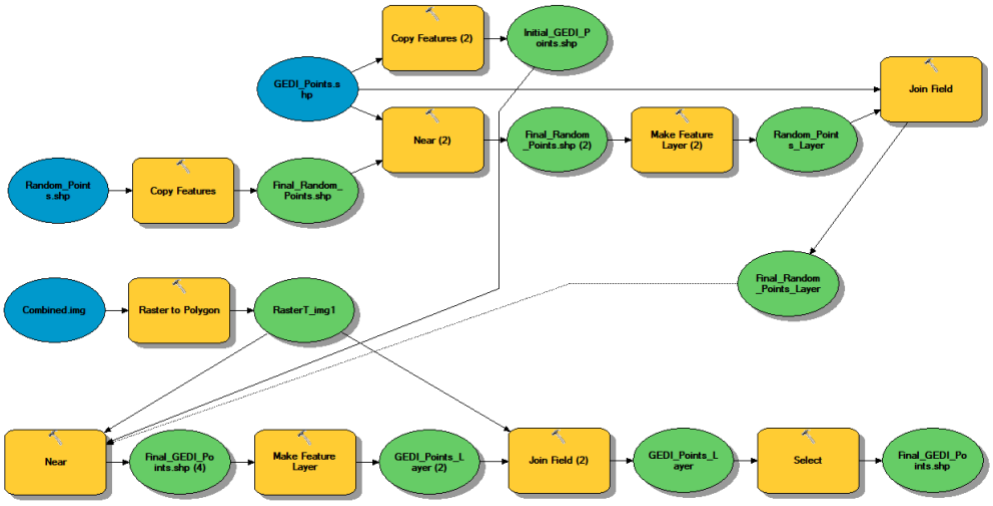

Figure 19. Model for calculating the distance from the center of fishnet cells to the nearest GEDI points.

Finally, the model was created for selecting random points for fieldwork plots (Figure 20), using the Python script (Appendix III).

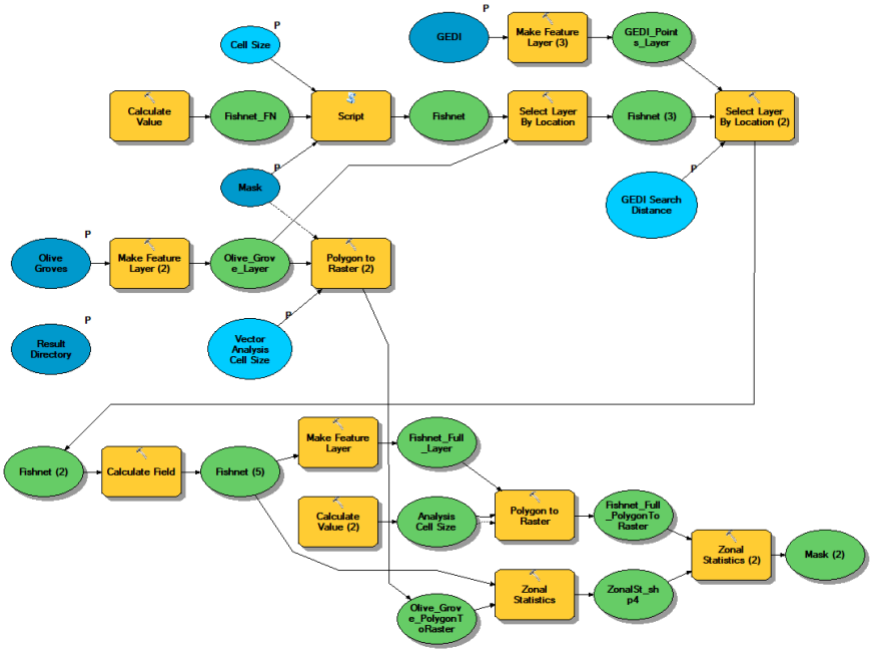

Figure 20. Final model for selecting random points for fieldwork plots.

This algorithm flow was used further for selecting 10 random points per category. These points were located in the field using a GPS device.

3.5. Field Data Collection

For carbon estimations, only aboveground living tree biomass was measured using non-destructive sampling, with allometric equations retrieved from variables. The methodology for field data gathering was proposed by Nikolaos Fyllas Research Group of the Department of the Environment, University of the Aegean, based on a variety of research literature and the personal experience of group members.

Plot-level information includes plot ID, region of the plot (Eastern, Central, Western Lesvos), date, coordinates of the plot center and four corners, elevation, aspect and slope degrees, and LAI data. The number of trees and all tree species were also recorded for each measured plot. Each tree height was measured using a measuring tape for measuring 10 m away from the tree to set up the point of observation, where the ruler was used for accessing the height of the tree. Basic information on the vegetation, land cover, the way of management (abandoned, low, mid, high), ground layer (low, mid, high), landscape homogeneity (low, mid, high) was also collected.

The accurate plot center coordinates and 4 plot corners including latitude and longitude were taken for each plot using a Google maps smartphone app (Google 2021). The slope was measured using a clinometer and Laser Level 1.5.02 (EXA Tools 2021) smartphone app.

3.5.1 LAI Estimation

LAI is a leaf area per unit of ground area. It was assessed using hemispherical photography as it is a common method to use for trees taller than 1.5 m (Veenendaal *et al.* 2015). It records the fraction of light below the canopy to the above canopy light.

LAI of plant canopy was derived using Decagon Accupar LAI Ceptometer portable sensor or a smartphone app VitiCanopy developed by a team from The University of Adelaide and The University of Melbourne (De Bei *et al.* 2016). A total of 30 samples were taken in each sample plot with 4 measurements from above each tree canopy.

3.5.2 Canopy Area Measurements

Canopy area is a sum of all tree crown areas on the plot. Tree crown was measured using a cross-method, which included measuring the longest spread from edge to edge and longest spread perpendicular to the first measurement using the measuring tape. The method is described in "Tree Measuring Guidelines of the Eastern Native Tree Society" (Blozan 2004).

Crown area was used for estimating canopy cover and predicting tree volume and biomass. In order to calculate it, the crown diameter is measured crosswise in two directions, the largest diameter and the diameter perpendicular to it (Figure 21).

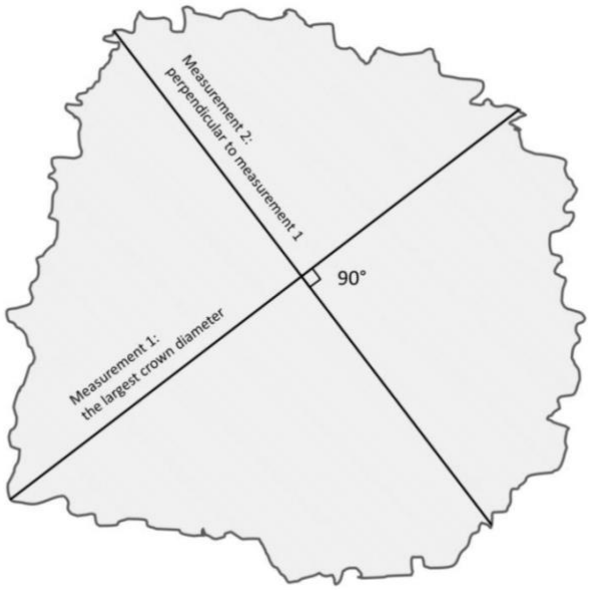

Figure 21. Measurement of crown diameter. The determination of the largest diameter is based on the visual assessment (Blozan 2004).

Crown area of trees for each plot was calculated as an area of an ellipse, using the following formula:

Crown area = longest spread * longest cross-spread * π / 4.

3.5.3 Stump Diameter Measurements

The average stump diameter (Ds) on the plot is the average diameter of the stumps of trees at a height of 30 cm from the surface. Within the plots, for each tree in the plot, the diameter at 30 cm above the ground was measured using a ruler.

The method for measuring tree stumps described in "Tree Measuring Guidelines of the Eastern Native Tree Society" (Blozan 2004) was used. In the case of the Blozan guideline, tree diameter was retrieved by measuring the DBH which is the height of 1.3 m above the ground level (Figure 22). In our case, measurements of the diameter of 0.3 m above the ground level were conducted since its higher predictive power.

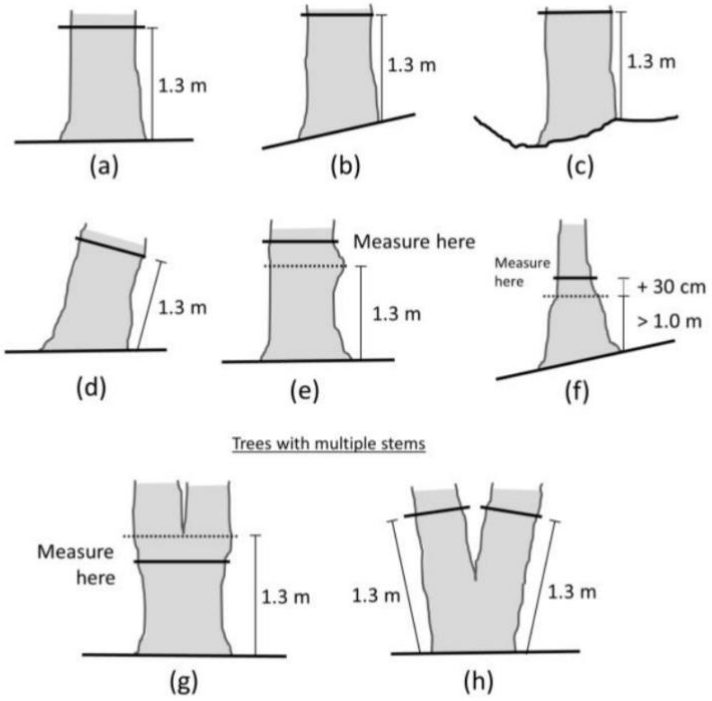

Figure 22. Measurement of DBH in different situations.
Level ground (a); slope (b), uneven ground (c); if the trunk is bent or inclined (d); if the tree has a limb, bulge or other abnormality (e); if the tree has buttresses (f); if tree forks exactly at breast height (g); if the tree has multiple stems (h) (Blozan 2004).

In total, 40 plots (30 x 30 m) were sampled and inventoried (Figures 23-28). These plots are part of all randomly generated plots. They were located in the field using a GPS device with errors up to 5 m.

Figure 23. Stump diameter measurements.

Figure 24. Setting plot borders.

Figure 25. LAI measurements.

Figure 26. DBH measurements.

Figure 27. Setting 90° angle for the plot corners.

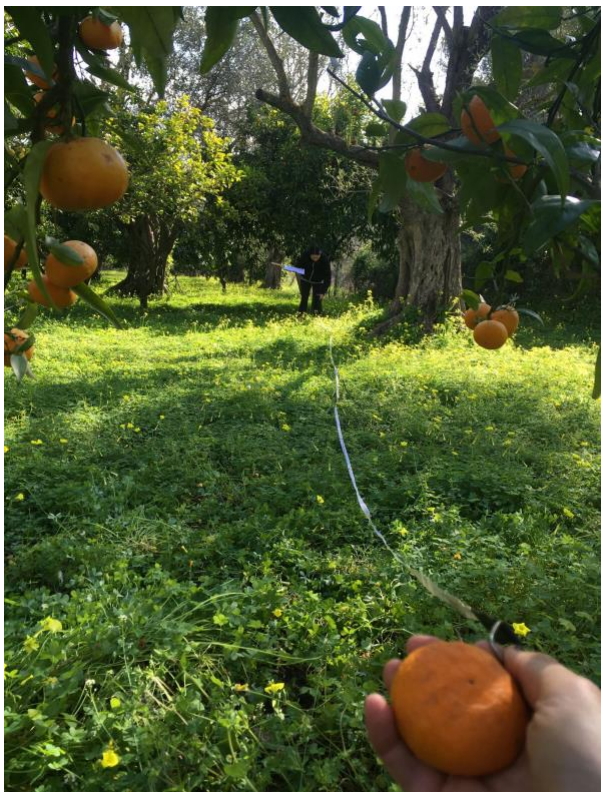

Figure 28. Tree height measurements.

3.6 Data Analysis

Python 3.7 (Pilgrim and Willison 2009) was used to download GEDI files for Lesvos and extract the data.

Python 3.7 and ArcMap 10.2.2 (ESRI 2014) were used to process the data from Landsat 8 and obtain VI from satellite images.

Statistical analysis was conducted by using the R statistical platform (R Core Team 2014).

For the retrieving equations which help to calculate total AGB on the plot, plot data were analysed with a simple linear regression analysis in R. To built algorithm flow for biomass, field data on LAI, Canopy Area (m2), average stump diameter (cm), number of trees (#/m2) was used.

For olive groves the generic equation predicting the total AGB from LAI was invented, equation based on field data for projecting data on PAI retrieved from GEDI points for the area of the olive grove on the island could be used. For calculating the AGCI, the conversion factor of 0.5 applied to the AGB was used.

A simple linear regression was used to calculate the correlation between canopy area and PAI, then average stump diameter and canopy area, number of trees and the average stump diameter, and, finally, total AGB and the number of trees and the average stump diameter.

Relationships between GEDI and Landsat data with field measurements were analysed using simple and multiple linear regression.

3.7. Strengths and Limitations

Among the strengths of the chosen methods, there are getting specific and detailed information about the specific location and chosen time frame, high representativeness, and the possibility to combine with other statistical and programming methods.

Among the limitations of these methods, there can be excessive damage in case of an internal fault, complex data structures, and issues connected with large amounts and complexity of data. Also, one of the main limitations of this approach is that biomass is not measured directly, by harvesting and weighing the leaves, branches, and stems of trees (Gonçalves *et al.* 2017).

3.8. Ethical Considerations

The research used quantitative methods so there were no ethical conflicts associated with the use of respondents. However, in relation to the research, many of the field work areas were fenced off as they are private agricultural areas. The members of the research group had to make their way to some closed areas, first asking permission from local farmers. Many fenced-in areas had to be avoided.

It was not implied that the research will be sponsored by external organizations, nor will it be supervised by external professionals and therefore external factors should not influence the course and results of the work.

Data was stored on a personal drive and duplicated on the OneDrive cloud service, provided by the Central European University. It is a safe and reliably protected service and therefore did not pose a danger to any actors involved in the research.

3.9. COVID-19 Impact

Travel restrictions on Lesvos island due to the COVID-19 outbreak prevented all field data from being collected by the end of the study programme, and the master's thesis field data was collected at 40 locations. However, the research work will continue until the end of 2021 and data for 108 points will be collected and analysed.

4. Results

4.1. Randomly Selected Points

Using the developed algorithm for selecting random points described in the Materials and Methods section, 10 random points per each of the 12 categories were selected (Figure 29). categories are described above in Table 2 in section Materials and Methods.

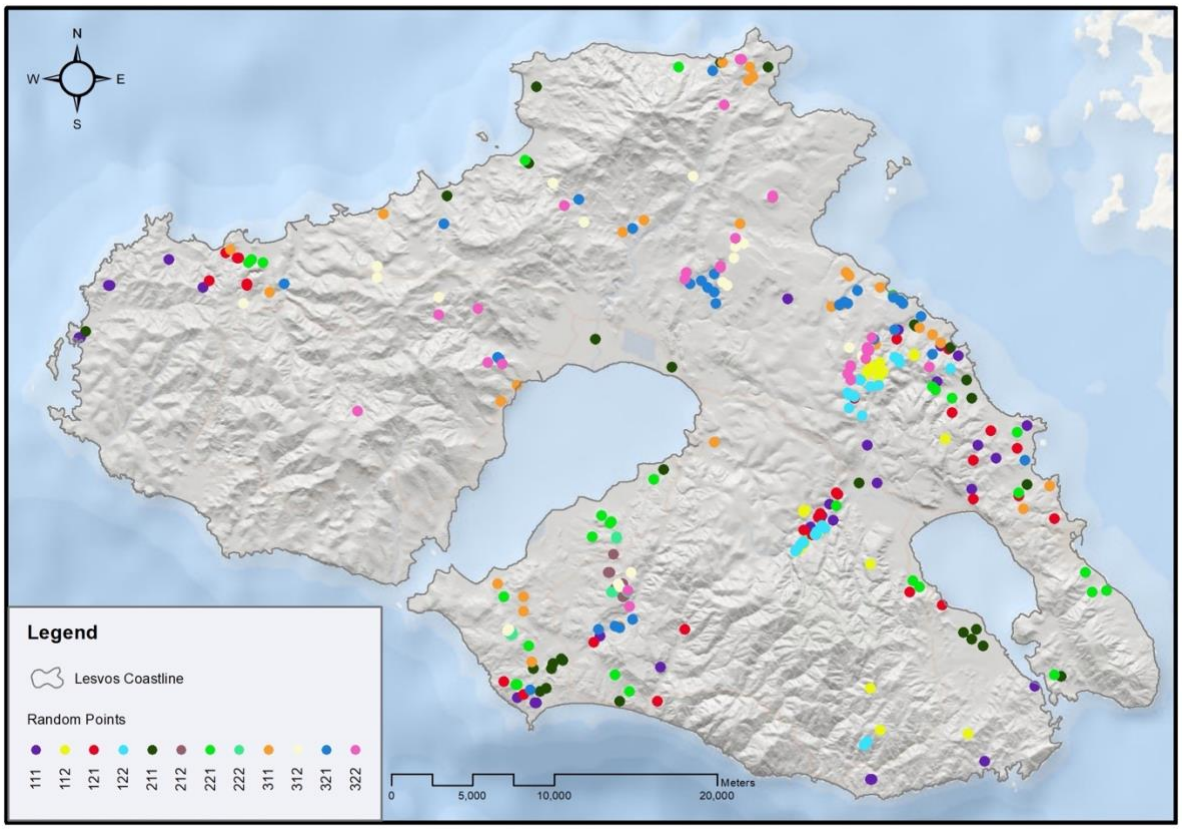

Figure 29. GEDI random points for conducting the fieldwork.

4.2. Field Work

Field work was carried out in accordance with the methodology described above in the Materials and Methods section. Due to restrictions related to COVID-19, data were obtained

from only 40 sites as a result. However, work on the project will continue and data for 108 sites will be collected by the end of the year.

Fyllas' Research Group developed an algorithm flow for estimating biomass based on field measurements (Figure 30).

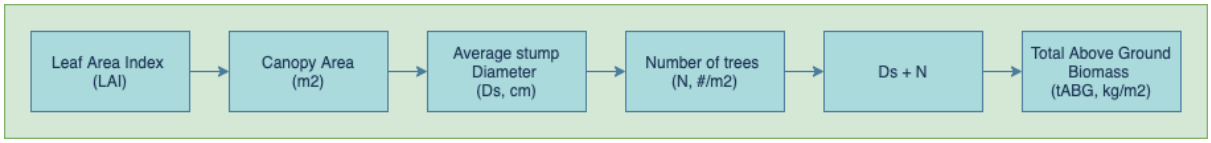

Figure 30. Algorithm flow for biomass estimation.

The following equations were achieved by a simple linear regression analysis:

Equations for average Canopy Area (m2):

if Elevation is less than 200 m, Elevation_Class = 0

if Elevation is more than 200 m, Elevation_Class = 1

if Slope is less than 7%, Slope_Class = 0

if Slope is more than 7%, Slope_Class = 1

CanArea = 18.665 + (20.687 * LAI) - (2.364 * Elevation_Class) - (5.366 * Slope_Class)

Equations for average stump Diameter (cm):

Ds = 36.2457+ (0.8371 * CanArea)

Equations for number of trees (#/m2):

N = (1/900) * exp(3.519229 - 0.013677 * Ds)

Equation for total AGB (kg DM / m2):

AGBt = N * (0.125 * Ds^2.279)

4.3. Statistical Analysis

After obtaining the data from the field work and GEDI products, the Landsat 8 Satellite Images were downloaded for GEDI point dates and dates of field work. Data on bands was retrieved and VI were calculated from spectral information using Python and analysed in R, with removing areas with clouds. For testing the correlation, the most common method of finding Pearson's r correlation coefficient was used in R, which measures the linear correlation between two sets of data. The correlation was tested between GEDI data on AGB and Landsat 8 bands and 7 chosen VI and field data on AGB and Landsat 8 bands and 7 chosen VI (Appendix V and VI).

Simple linear regression analysis was conducted for each band and each indices and multiple linear regression analysis was conducted for different combinations of bands and indices. Analysis was conducted for all the available dates of satellite data.

Data obtained on statistical significance (p-value) and correlation (Adjusted R-squared) did not show any significance and correlation (Figures 31 and 32).

	y	x1	x2	x3	x4	x5	x6	x7	x10	NDVI	IRVI	RVI	GNDVI	SAVI	TVI	EVI
y	1.00	-0.18	-0.20	-0.22	-0.21	-0.05	-0.26	-0.24	-0.12	0.07	-0.07	0.07	0.05	0.07	0.07	0.20
x1	-0.18	1.00	0.98	0.88	0.93	0.19	0.88	0.92	0.65	-0.30	0.31	-0.29	-0.18	-0.30	-0.30	-0.50
x2	-0.20	0.98	1.00	0.92	0.97	0.17	0.89	0.94	0.64	-0.34	0.35	-0.33	-0.22	-0.34	-0.34	-0.55
x3	-0.22	0.88	0.92	1.00	0.93	0.44	0.90	0.88	0.66	-0.08	0.09	-0.06	0.03	-0.08	-0.08	-0.61
x4	-0.21	0.93	0.97	0.93	1.00	0.15	0.89	0.95	0.61	-0.38	0.39	-0.37	-0.25	-0.38	-0.38	-0.63
x5	-0.05	0.19	0.17	0.44	0.15	1.00	0.35	0.13	0.50	0.85	-0.84	0.86	0.90	0.85	0.85	-0.22
x6	-0.26	0.88	0.89	0.90	0.89	0.35	1.00	0.95	0.71	-0.13	0.13	-0.13	-0.01	-0.13	-0.13	-0.61
x7	-0.24	0.92	0.94	0.88	0.95	0.13	0.95	1.00	0.64	-0.37	0.37	-0.36	-0.24	-0.37	-0.37	-0.60
x10	-0.12	0.65	0.64	0.66	0.61	0.50	0.71	0.64	1.00	0.17	-0.17	0.15	0.28	0.17	0.17	-0.46
NDVI	0.07	-0.30	-0.34	-0.08	-0.38	0.85	-0.13	-0.37	0.17	1.00	-1.00	0.99	0.99	1.00	1.00	0.10
IRVI	-0.07	0.31	0.35	0.09	0.39	-0.84	0.13	0.37	-0.17	-1.00	1.00	-0.98	-0.98	-1.00	-1.00	-0.09
RVI	0.07	-0.29	-0.33	-0.06	-0.37	0.86	-0.13	-0.36	0.15	0.99	-0.98	1.00	0.97	0.99	0.98	0.10
GNDVI	0.05	-0.18	-0.22	0.03	-0.25	0.90	-0.01	-0.24	0.28	0.99	-0.98	0.97	1.00	0.99	0.99	-0.01
SAVI	0.07	-0.30	-0.34	-0.08	-0.38	0.85	-0.13	-0.37	0.17	1.00	-1.00	0.99	0.99	1.00	1.00	0.10
TVI	0.07	-0.30	-0.34	-0.08	-0.38	0.85	-0.13	-0.37	0.17	1.00	-1.00	0.98	0.99	1.00	1.00	0.09
EVI	0.20	-0.50	-0.55	-0.61	-0.63	-0.22	-0.61	-0.60	-0.46	0.10	-0.09	0.10	-0.01	0.10	0.09	1.00

Figure 31. Results of correlation analysis between GEDI data and Landsat 8 images for April 1, 2019, where y is GEDI data on AGB, x1-x10 are Landsat 8 bands, and NDVI, IRVI, RVI, GNDVI, SAVI, TVI, and EVI are tested VI.

	y	x1	x2	x3	x4	x5	x6	x7	x10	NDVI	IRVI	RVI	GNDVI	SAVI	TVI	EVI
y	1.00	0.00	0.00	-0.01	-0.01	0.04	-0.10	-0.04	0.04	0.04	-0.04	0.03	0.04	0.04	0.04	0.05
x1	0.00	1.00	0.99	0.90	0.95	-0.01	0.87	0.92	0.77	-0.56	0.57	-0.54	-0.51	-0.56	-0.56	-0.73
x2	0.00	0.99	1.00	0.93	0.98	0.02	0.90	0.95	0.78	-0.55	0.57	-0.53	-0.49	-0.55	-0.56	-0.80
x3	-0.01	0.90	0.93	1.00	0.94	0.32	0.90	0.87	0.75	-0.28	0.30	-0.25	-0.22	-0.28	-0.29	-0.84
x4	-0.01	0.95	0.98	0.94	1.00	0.01	0.90	0.96	0.73	-0.57	0.59	-0.55	-0.51	-0.57	-0.58	-0.89
x5	0.04	-0.01	0.02	0.32	0.01	1.00	0.19	-0.06	0.25	0.82	-0.80	0.83	0.85	0.82	0.81	-0.09
x6	-0.10	0.87	0.90	0.90	0.90	0.19	1.00	0.95	0.75	-0.36	0.37	-0.35	-0.29	-0.36	-0.37	-0.81
x7	-0.04	0.92	0.95	0.87	0.96	-0.06	0.95	1.00	0.74	-0.60	0.61	-0.58	-0.53	-0.60	-0.61	-0.85
x10	0.04	0.77	0.78	0.75	0.73	0.25	0.75	0.74	1.00	-0.21	0.22	-0.20	-0.15	-0.21	-0.22	-0.53
NDVI	0.04	-0.56	-0.55	-0.28	-0.57	0.82	-0.36	-0.60	-0.21	1.00	-1.00	1.00	0.99	1.00	1.00	0.45
IRVI	-0.04	0.57	0.57	0.30	0.59	-0.80	0.37	0.61	0.22	-1.00	1.00	-0.99	-0.99	-1.00	-1.00	-0.47
RVI	0.03	-0.54	-0.53	-0.25	-0.55	0.83	-0.35	-0.58	-0.20	1.00	-0.99	1.00	0.99	1.00	0.99	0.41
GNDVI	0.04	-0.51	-0.49	-0.22	-0.51	0.85	-0.29	-0.53	-0.15	0.99	-0.99	0.99	1.00	0.99	0.99	0.38
SAVI	0.04	-0.56	-0.55	-0.28	-0.57	0.82	-0.36	-0.60	-0.21	1.00	-1.00	1.00	0.99	1.00	1.00	0.45
TVI	0.04	-0.56	-0.56	-0.29	-0.58	0.81	-0.37	-0.61	-0.22	1.00	-1.00	0.99	0.99	1.00	1.00	0.46
EVI	0.05	-0.73	-0.80	-0.84	-0.89	-0.09	-0.81	-0.85	-0.53	0.45	-0.47	0.41	0.38	0.45	0.46	1.00

Figure 32. Results of correlation analysis between field data and Landsat 8 images for April 1, 2019, where y is field data on AGB, x1-x10 are Landsat 8 bands, and NDVI, IRVI, RVI, GNDVI, SAVI, TVI, and EVI are tested VI.

For GEDI and Landsat regression analysis, the scatterplots show some intense clustering of values for most of the bands and VI (Figure 33). This clustering can be further investigated using multidimensional clustering techniques, such as, for example, the most popular k-means clustering method.

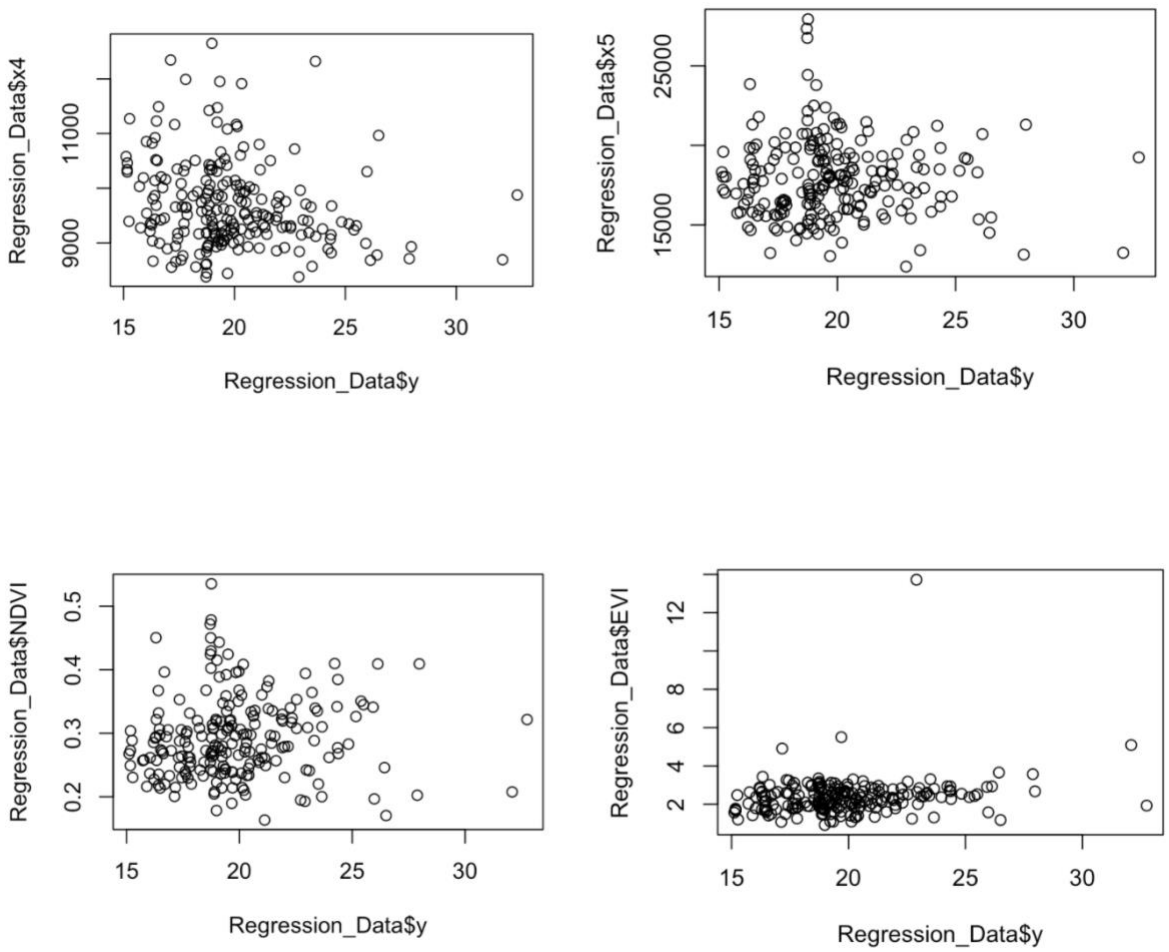

Figure 33. Regression analysis Scatter Plots
between GEDI data and Landsat 8 Band 4 (Red), Band 5 (NIR), NDVI, and EVI for April 1, 2019.

4.3. AGB and AGCI Mapping

AGB and AGCI estimations for GEDI points were calculated from the PAI value using the algorithm described above. To interpolate data of GEDI points to the area of olive groves on Lesvos, two interpolation methods were applied, simple Kriging and Inverse distance weighting (IDW). By masking the interpolation results to olive groves, maps for the amount of AGB and carbon stocks were created (Figures 34-37) and then the biomass and carbon stocks values were calculated for the area of olive groves.

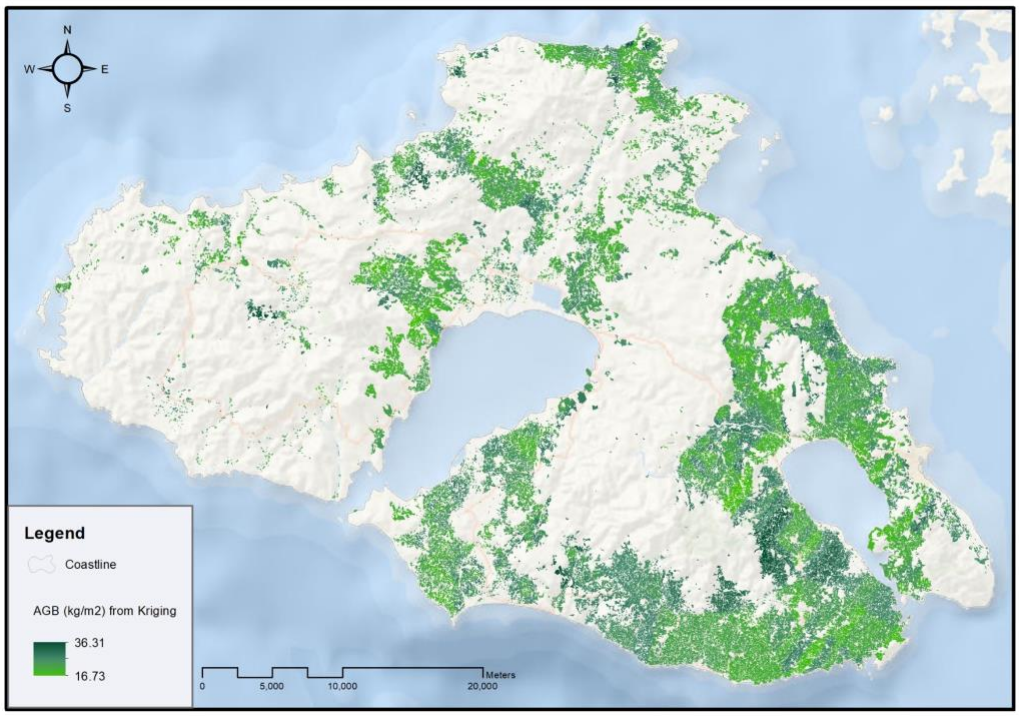

Figure 34. AGB map of Lesvos olive groves created by using the Kriging method.

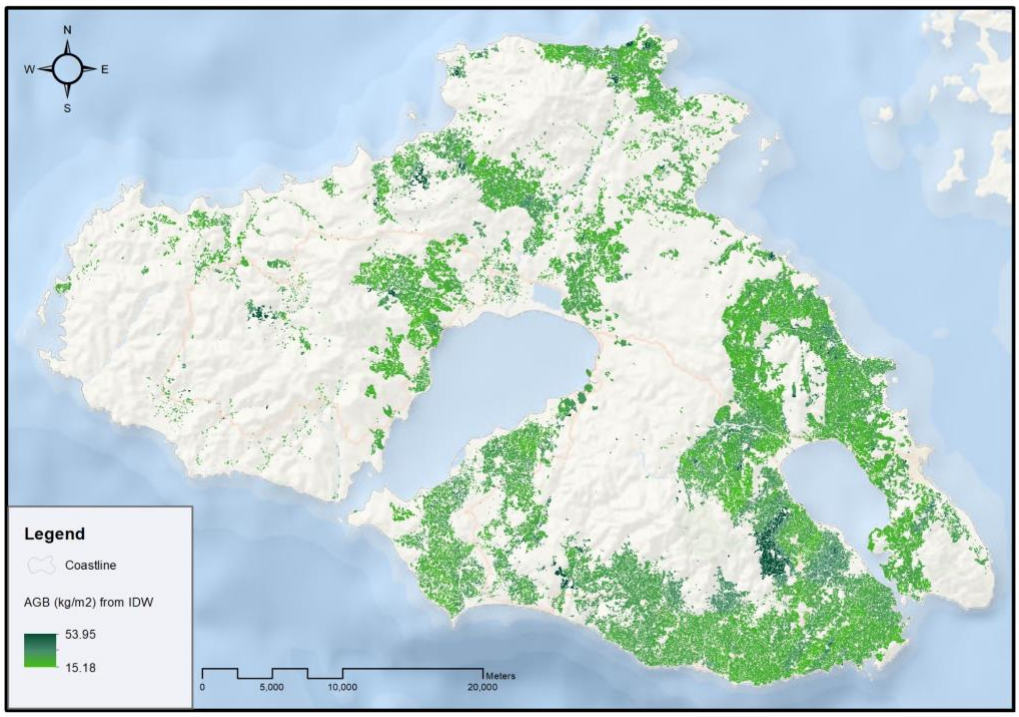

Figure 35. AGB map of Lesvos olive groves created by using the IDW method.

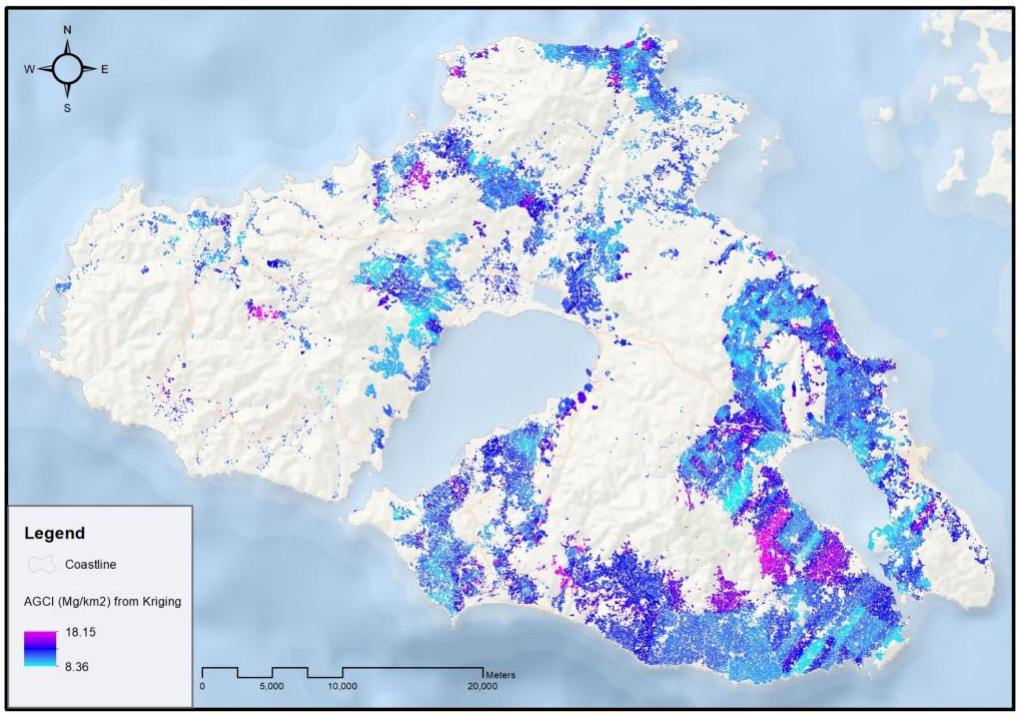

Figure 36. AGCI map of Lesvos olive groves created by using the Kriging method.

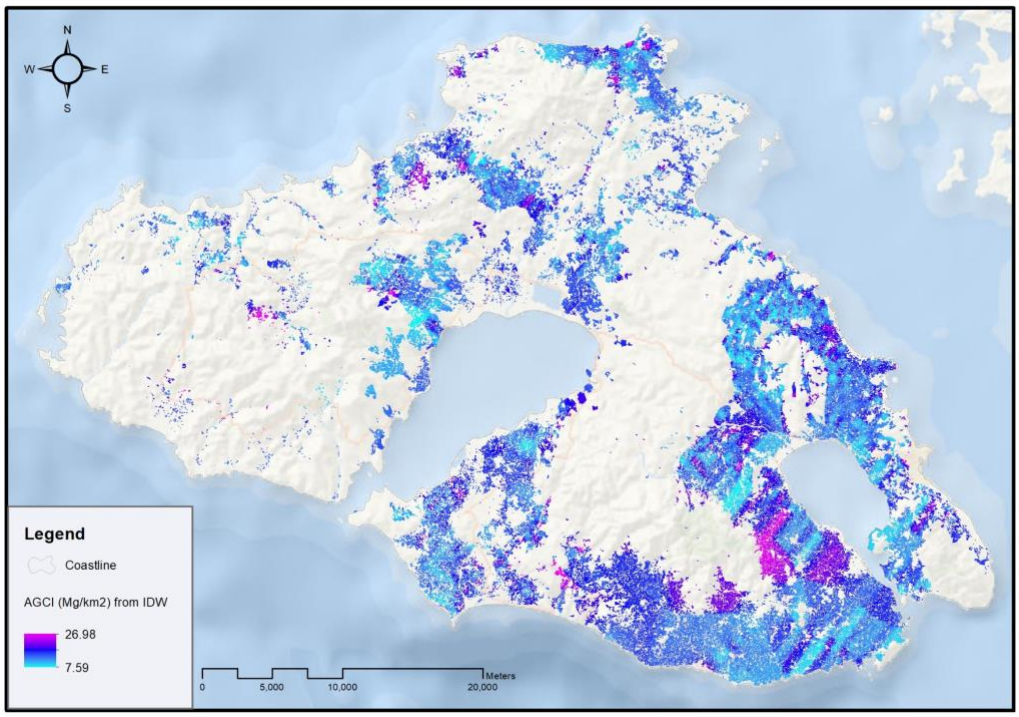

Figure 37. AGCI map of Lesvos olive groves created by using the IDW method.

Using Zonal Statistics tool, total AGB and AGCI of Lesvos olive groves were calculated. According to the Kriging method, the total AGB of Lesvos olive groves is 8.151 billion kg. IDW showed a similar result, 8.155 billion kg.

AGCI from Kriging showed a predictable result of 4.075 billion, which is half number of AGB estimation. IDW, consequently, showed a result of 4.077 billion.

5. Discussion

5.1. General Discussion

According to the correlation analysis between Landsat 8 Bands and VI and GEDI data, and Landsat 8 Bands and VI and field biomass estimations, there is no linear correlation discovered. At the beginning of the research, Pearson's r between PAI values from GEDI and LAI from fieldwork, as well as biomass estimations retrieved from PAI and LAI values, was around 0.7 for 20 plots and downgraded to around 0.45 for 40 plots. However, more field trips are expected and this value may change later with obtaining more results from the field work and updating the equation for biomass estimation from the LAI indicator. Updating the equation can lead to better correlation results between field and Landsat 8 derived data.

Possible reasons for the lack of correlation can be the spatial accuracy of GEDI data and the failure of GEDI to capture accurate PAI values in less dense forests such as olive groves. The aim of GEDI as it claimed is to enhance large-scale forest maps. GEDI LiDAR data was used for tropical forest and global forest mapping (Dubayah 2020; Potapov *et al.* 2021; Tang and Armston 2019) and deciduous and conifer forests (Adam *et al.* 2020; Chen *et al.* 2021; Guerra-Hernández and Pascual 2021). However, GEDI data was not used for agricultural lands.

Guerra-Hernández and Pascual (2021) highlight that errors in GEDI data can come from positioning, ground finder, and estimating canopy structure for GEDI. The analysis of biomass of olive groves would benefit by using more extensive field observations, and adjusting GEDI data settings precisely for PAI on agricultural groves.

The developed method of sampling random points for field work can be used for subsequent research. The proposed biomass and carbon estimates based on GEDI data and

fieldwork can be used to inform policy makers regarding agricultural management at the regional level.

5.2. Implications and Policy Recommendations

Greece has a target for carbon intensity reduction (EC 2019), however, objectives of research and innovation are unclear now for the period after 2020. To set the objectives, Greek policy makers should use science-based information for decision-making regarding carbon stocks. Results obtained in this thesis can be used as one of the milestones in understanding and developing the correct methodology for estimating biomass and therefore carbon stocks.

The results can also be useful in the development of management proposals for sustainable olive groves agriculture. As a result of MESPOM (2020) research group work on the effects of climate change on Lesvos' olive production, Campaign for Carbon Neutrality was offered. To start developing the campaign, the initial step is to assess existing carbon stocks and identify the best strategy for estimating biomass. There is a need to improve the methodology for estimating biomass using GIS tools, RS, and LiDAR data, as field work is very labor-intensive, expensive, and time-consuming.

Among policy recommendations, it is worth emphasizing the necessity of creating a clear and user-friendly information hub on carbon stocks, for Greece and specifically Lesvos, for forests in general, and for olive groves in particular. The creation, supporting, and timely updating of such a hub with clear information on sustainable farming, as well as implementing leverages for farmers, can help to conduct more sustainable agriculture aimed at storing more carbon and increase the potential storage volume of olive trees as an additional ES.

Lesvos can be used as a pilot area due to the developed olive farming and big farmers' community. Farmers might use the information from the hub for achieving more precise

information on the adoption of new cultivars, more sustainable ways of pruning, and necessary changes in farmers' training. Lesvos's experience can be applied to agricultural management in Greece and the Mediterranean region.

6. Conclusion

The principal aim of the thesis research was to examine the ability of LiDAR data and satellite imagery to estimate AGB and carbon stocks of olive groves on Lesvos Island, Greece. For the research, the most commonly used satellite data (Landsat 8) and relatively new LiDAR data (GEDI) have been assessed for developing the methodology for biomass and carbon stocks monitoring.

The research showed the potential of using data retrieved from the GEDI product L2B for assessing and mapping biomass and carbon stocks of olive groves on Lesvos island, Greece. LAI and PAI values were retrieved from field data and GEDI and tested for correlation with Landsat 8. Although correlation and regression analysis between Landsat data and GEDI and fieldwork data did not show linear correlation, the GEDI data has potential in biomass and carbon stocks estimation, along with a combination of other RS technologies and field observations. The results show a necessity for continuation of field work for further development of methodology for remote biomass estimation.

Maps on biomass and carbon stocks of olive groves on Lesvos were created and values on AGB and carbon stocks indicators were obtained. With the continuation of the fieldwork and finishing the project, updated results can be used by policy makers for science-based decision-making in developing a more sustainable agriculture system aimed to store more carbon in agricultural groves at the local and regional levels.

Bibliography

Adam, M., Urbazaev, M., Dubois, C., and Schmullius, C. 2020. Accuracy Assessment of GEDI Terrain Elevation and Canopy Height Estimates in European Temperate Forests: Influence of Environmental and Acquisition Parameters. *Remote Sensing* 12 (23): 3948.

Aguilera, F. and Ruiz-Valenzuela, L. 2014. Forecasting olive crop yields based on long-term aerobiological data series and bioclimatic conditions for the southern Iberian Peninsula. *Spanish Journal of Agricultural Research* 12 (1): 215.

Alcamo, J., Hassan, R., Scholes, R., Ash, N., Carpenter, S. R., Pingali, P. L., Raudsepp-Hearne, C. 2005. *Ecosystems and human well-being.* Vol. 4: Multiscale assessments: findings of the Sub-global Assessments Working Group of the Millenium Ecosystem Assessment.

Asner, G. P. and Mascaro, J. 2014. Mapping tropical forest carbon: Calibrating plot estimates to a simple LiDAR metric. *Remote Sensing of Environment* 140: 614–624.

Beaufoy, G. 2001. The Environmental Impact Of Olive Oil Production In The European Union: Practical Options For Improving The Environmental Impact. Peterborough, United Kingdom; Madrid, Spain: European Forum on Nature Conservation and Pastoralism and the Análisis y Reforma de la Política Agro-rural (ENAMA). Accessed March 19. URL: http://www.efncp.org/download/oliveoil.pdf

Bergen, K. M. and Dobson, M. Craig. 1999. Integration of remotely sensed radar imagery in modeling and mapping of forest biomass and net primary production. *Ecological Modelling* 122 (3): 257–274.

Blozan, W. 2004. *Tree Measuring Guidelines of the Eastern Native Tree Society*. Accessed March 20. URL: http://apps.worldagroforestry.org/downloads/Publications/PDFS/RP16065.pdf

Boisvenue, C., Smiley, B. P., White, J. C., Kurz, W. A., and Wulder, M. A. 2016. Integration of Landsat time series and field plots for forest productivity estimates in decision support models. *Forest Ecology and Management* 376: 284–297.

Brilli, L., Lugato, E., Moriondo, M., Gioli, B., Toscano, P., Zaldei, A., … Costafreda-Aumedes, S. 2018. Carbon sequestration capacity and productivity responses of Mediterranean olive groves under future climates and management options. *Mitigation and Adaptation Strategies for Global Change* 24 (3): 467–491.

Brockett, B. F. T., Browne, A. L., Beanland, A., Whitfield, M. G., Watson, N., Blackburn, G. A., and Bardgett, R. D. 2019. Guiding carbon farming using interdisciplinary mixed methods mapping. *People and Nature* 3 (24).

Brunori, E., Maesano, M., Moresi, F.V., Matteucci, G., Biasi, R., and Mugnozza, G.S. 2019. The hidden land conservation benefits of olive-based (*Olea europaea* L.) landscapes: An agroforestry investigation in the southern Mediterranean (Calabria region, Italy). *Land Degradation and Development* 31 (7): 801-815.

Buckwell, A., Matthews, A., Baldock, D., and Mathijs, E. 2017. *CAP – Thinking Out of the Box: Further modernisation of the CAP – why, what and how?* Brussels: RISE Foundation. Accessed April 22. URL: https://lirias.kuleuven.be/1742627

Castro, J., Fernández-Ondoño, E., Rodríguez, C., Lallena, A., Sierra, M. and Aguilar, J., 2008. Effects of different olive-grove management systems on the organic carbon and nitrogen content of the soil in Jaén (Spain). *Soil and Tillage Research* 98 (1): 56-67.

Chave, J., Andalo, C., Brown, S., Cairns, M. A., Chambers, J. Q., Eamus, D., … Yamakura, T. 2005. Tree allometry and improved estimation of carbon stocks and balance in tropical forests. *Oecologia* 145 (1): 87–99.

Chave, J., Réjou-Méchain, M., Búrquez, A., Chidumayo, E., Colgan, M. S., Delitti, W. B. C., … Pélissier, R. 2014. Improved allometric models to estimate the aboveground biomass of tropical trees. *Global Change Biology* 20 (10): 3177–3190.

Chen, J. M., and Black, T. A. 1992. Defining leaf area index for non-flat leaves. *Plant, Cell and Environment* 15 (4): 421–429.

Chen, L., Ren, C., Zhang, B., Wang, Z., Liu, M., Man, W., and Liu, J. 2021. Improved estimation of forest stand volume by the integration of GEDI LiDAR data and multi-sensor imagery in the Changbai Mountains Mixed forests Ecoregion (CMMFE), northeast China. *International Journal of Applied Earth Observation and Geoinformation* 100 (10): 23-26.

Coderoni, S., Longhitano, D., and Vinci, A. 2014. Payment for Ecosystem Service for Carbon Credits from Italian Olive Groves. Some Issues Regarding the Mode of Payment. *International Journal of Food and Agricultural Economics (IJFAEC)* 2 (4).

Corral-Rivas, J. J., Barrio-Anta, M., Aguirre-Calderon, O. A., and Dieguez-Aranda, U. 2007. Use of stump diameter to estimate diameter at breast height and tree volume for major pine species in El Salto, Durango (Mexico). *Forestry* 80 (1): 29–40.

De Bei, R., Fuentes, S., Gilliham, M., Tyerman, S., Edwards, E., Bianchini, N., … Collins, C. 2016. VitiCanopy: A Free Computer App to Estimate Canopy Vigor and Porosity for Grapevine. *Sensors* 16 (4): 585.

Department of Agriculture, Region of North Aegean. 2020. Pomace production Lesvos 2019-2020. Accessed March 25. URL: http://www.ptaba.gr/dyn/banner/061215142847_b.pdf

Dios-Palomares, R. and Martínez-Paz, J. M. 2011. Technical, quality and environmental efficiency of the olive oil industry. *Food Policy* 36 (4): 526–534.

Drake, J. B., Knox, R. G., Dubayah, R. O., Clark, D. B., Condit, R., Blair, J. B., and Hofton, M. 2003. Above-ground biomass estimation in closed canopy Neotropical forests using lidar remote sensing: factors affecting the generality of relationships. *Global Ecology and Biogeography* 12 (2): 147–159.

Dubayah, R., Blair, J. B., Goetz, S., Fatoyinbo, L., Hansen, M., Healey, S., … Silva, C. 2020. The Global Ecosystem Dynamics Investigation: High-resolution laser ranging of the Earth's forests and topography. *Science of Remote Sensing* 1: 100002.

Dubayah, R., Tang, H., Armston, J., Luthcke, S., Hofton, M., Blair, J. 2020. *GEDI L2B Canopy Cover and Vertical Profile Metrics Data Global Footprint Level V001* [Data set]. NASA EOSDIS Land Processes DAAC. Accessed February 15. URL: https://doi.org/10.5067/GEDI/GEDI02_B.001

Du, L., Zhou, T., Zou, Z., Zhao, X., Huang, K., and Wu, H. 2014. Mapping Forest Biomass Using Remote Sensing and National Forest Inventory in China. *Forests* 5 (6): 1267–1283.

Elhag, M., Boteva, S., and Al-Amri, N. 2021. Forest cover assessment using remote-sensing techniques in Crete Island, Greece. *Open Geosciences* 13(1): 345–358.

Environmental Systems Research Institute (ESRI). 2014. ArcGIS Desktop Help 10.2 Geostatistical Analyst.

Erasmus Mundus Joint Master Degree in Environmental Sciences, Policy and Management (MESPOM). 2020. *The Olive Land Use System of Lesvos: Status and Ecosystem Management Options. Group Report for Assessment, Modelling, and Scenarios for Ecosystems Management course*. Department of Environment, University of the Aegean, Mytilene, Greece. Duplicated.

European Commission (EC). 2018. DOPA factsheet on aboveground carbon. Accessed April 30. URL: https://dopa.jrc.ec.europa.eu/sites/default/files/DOPA%20Factsheet%20J2%20Above%20Ground%20Carbon_0.pdf

_____. 2019. Summary of the Commission assessment of the draft of Greek National Energy and Climate Plan 2021-2030. Accessed April 15. URL: https://ec.europa.eu/energy/sites/ener/files/documents/necp_factsheet_el_final.pdf

_____. 2020. Balance Sheet: Olive Oil. Accessed April 25. URL: https://ec.europa.eu/info/sites/info/files/food-farming-fisheries/plants_and_plant_products/documents/olive-oil-balance-sheet_fr.pdf

EXA Tools. 2019. Laser Level. Version 1.5.02. Accessed February 28. URL: https://play.google.com/store/apps/details?id=com.exatools.laserlevel

Food and Agriculture Organization of the United Nations (FAO). 2015. Soils Help To Combat And Adapt To Climate Change By Playing A Key Role In The Carbon Cycle. Rome: Italy. Accessed February 22. URL: http://www.fao.org/3/a-i4737e.pdf.

Fernández-Habas, J., Sánchez-Zamora, P., Ceña-Delgado, F., and Gallardo-Cobos, R. 2018. Assessment of ecosystem services provision: The case of mountain olive groves in Los Pedroches, Southern Spain. *New Medit* 17 (2): 43–60.

Fleskens, L. 2007. Conservation Scenarios for Olive Farming on Sloping Land in the Mediterranean, Chapter 3: A Typology of Sloping and Mountainous Olive Plantation Systems to Address Natural Resources Management. Ph.D Thesis, Wageningen University, Wageningen, Netherlands. Accessed March 12. URL: https://edepot.wur.nl/44120

Galán, C., García-Mozo, H., Vázquez, L., Ruiz, L., De La Guardia, C. D., and Trigo, M.M. 2005. Heat requirement for the onset of the *Olea europaea* L. pollen season in several sites in Andalusia and the effect of the expected future climate change. *International Journal of Biometeorology* 49: 184–188.

Georgopoulou, E., Mirasgedis, S., Sarafidis, Y., Vitaliotou, M., Lalas, D. P., Theloudis, I., Giannoulaki, K.-D., Dimopoulos, D., and Zavras, V. 2017. Climate change impacts and adaptation options for the Greek agriculture in 2021–2050: A monetary assessment. *Climate Risk Management* 16: 164-182.

Giorgi, F. 2006. Climate change hot-spots. *Geophysical Research Letters* 33: 8707.

Giourga, C., Loumou, A., Tsevreni, I., and Vergou, A. 2008. Assessing the sustainability factors of traditional olive groves on Lesvos Island, Greece. *GeoJournal* 73 (2): 149–159.

Gitelson, A. 2004. Wide Dynamic Range Vegetation Index for Remote Quantification of Biophysical Characteristics of Vegetation. *Journal of Plant Physiology* 161 (2): 165–173.

Gonçalves, F., Treuhaft, R., Law, B., Almeida, A., Walker, W., Baccini, A., … Graça, P. 2017. Estimating Aboveground Biomass in Tropical Forests: Field Methods and Error Analysis for the Calibration of Remote Sensing Observations. *Remote Sensing* 9(1): 47.

Google. 2019. *Google Maps app*. Accessed May 12. URL: https://www.google.gr/maps.

Guerra-Hernández, J. and Pascual, A. 2021. Using GEDI lidar data and airborne laser scanning to assess height growth dynamics in fast-growing species: a showcase in Spain. *Forest Ecosystems* 8 (1).

Gutierrez, A. P., Ponti, L., and Cossu, Q. A. 2009. Effects of climate warming on Olive and olive fly Bactrocera oleae (Gmelin) in California and Italy. *Climatic Change* 95 (1–2): 195–217.

Han, L., Yang, G., Dai, H., Xu, B., Yang, H., Feng, H., … Yang, X. 2019. Modeling maize above-ground biomass based on machine learning approaches using UAV remote-sensing data. *Plant Methods* 15 (1).

Hellenic Agricultural Enterprises. 2020. *Importance of olive production on Lesvos*. Accessed March 21. URL: http://www.hae-gr.com/lesvos.php

Höhnel, P. 2019. Oleo-Ceratonion. Seminar contribution to the module Terrestrial Ecosystems, Institute of Botany, University of Hohenheim, Stuttgart. Accessed March 12. URL: https://botanik.uni-hohenheim.de/fileadmin/einrichtungen/botanik/exkursion_i/2019_Nordzypern/2019_14_Oleo-Ceratonion.pdf

Hudak, A. T., Lefsky, M. A., Cohen, W. B., and Berterretche, M. 2002. Integration of lidar and Landsat ETM+ data for estimating and mapping forest canopy height. *Remote Sensing of Environment* 82 (2-3): 397–416.

Hyyppä, J., Hyyppä, H., Inkinen, M., Engdahl, M., Linko, S., and Zhu, Y.-H. 2000. Accuracy comparison of various remote sensing data sources in the retrieval of forest stand attributes. *Forest Ecology and Management* 128 (1-2): 109–120.

Intergovernmental Panel On Climate Change (IPCC). 2013. Climate Change 2013: The physical science basis. Contribution of working group I to the Fifth Assessment Report of the Intergovernmental Panel on Climate Change. Cambridge University Press, Cambridge, United Kingdom and New York, NY, USA.

_____. 2015. Climate Change 2014: Synthesis Report: Contribution of working groups I, II and III to the Fifth Assessment Report of the Intergovernmental Panel on Climate Change. Geneva, Switzerland: IPCC.

_____. 2018. Global warming of 1.5°C: an IPCC special report on the impacts of global warming of 1.5°C above pre-industrial levels and related global greenhouse gas emission pathways, in the context of strengthening the global response to the threat of climate change, sustainable development, and efforts to eradicate poverty. Geneva, Switzerland: IPCC.

_____. 2019. IPCC Assessment Report 2019. Geneva, Switzerland: IPCC.

International Olive Council. 2015. International Olive Oil Production Costs Study. Accessed May 2. URL: https://www.internationaloliveoil.org/wp-content/uploads/2019/11/international-olive-oil-production-costs-study-.pdf

Janssens, I. A. 2003. Europe's Terrestrial Biosphere Absorbs 7 to 12% of European Anthropogenic CO2 Emissions. *Science* 300 (5625): 1538–1542.

Jensen, J., Humes, K., Vierling, L., and Hudak, A. 2008. Discrete return lidar-based prediction of leaf area index in two conifer forests. *Remote Sensing of Environment*, 112 (10): 3947–3957.

Jiménez-Alfaro, B., Frischie, S., Stolz, J., and Gálvez-Ramírez, C. 2020. Native plants for greening Mediterranean agroecosystems. *Nature Plants* 6 (3): 209-214.

Kebede, B. and Soromessa, T. 2018. Allometric equations for aboveground biomass estimation of *Olea europaea* L. subsp. *cuspidata* in Mana Angetu Forest. *Ecosystem Health and Sustainability* 4 (1): 1–12.

Keith, H., Vardon, M., Lindenmayer, D., and Mackey, B. 2019. Accounting for carbon stocks and flows: storage and sequestration are both ecosystem services. *The 25th Meeting of the London Group on Environmental Accounting*. Accessed May 20. URL: https://seea.un.org/sites/seea.un.org/files/carbon_accounts_london_group_oct_2019_h keith.pdf

Kizos, T. and Vakoufaris, H. 2011. Valorisation of a local asset: The case of olive oil on Lesvos Island, Greece. *Food Policy* 36(5): 705–714.

Ladisa, G., Calabre, G., and Perrino, E. V. 2012. The origin and distribution of olive trees and olive crop. Study on biodiversity in century-old olive groves. CIHEAM: Mediterranean Agronomic Institute of Bari. Accessed March 18. URL: https://www.researchgate.net/publication/254256636

Lima-Cueto, F. J., Blanco-Sepúlveda, R., Gómez-Moreno, M. L., and Galacho-Jiménez, F. B. 2019. Using Vegetation Indices and a UAV Imaging Platform to quantify the density of vegetation ground cover in olive groves (*Olea europaea* L.) in Southern Spain. *Remote Sensing* 11 (21): 2564.

Li, N., Xie, G., Zhang, C., Xiao, Y., Zhang, B., Chen, W., … Wang, S. 2015. Biomass Resources Distribution in the Terrestrial Ecosystem of China. *Sustainability* 7 (7): 8548–8564.

Li, Y., Li, M., Li, C., and Liu, Z. 2020. Forest aboveground biomass estimation using Landsat 8 and Sentinel-1A data with machine learning algorithms. *Scientific Reports* 10(1).

López-Serrano, P., Corral-Rivas, J., Díaz-Varela, R., Álvarez-González, J., and López-Sánchez, C. 2016. Evaluation of Radiometric and Atmospheric Correction Algorithms for Aboveground Forest Biomass Estimation Using Landsat 5 TM Data. *Remote Sensing* 8 (5): 369.

López-Serrano, P. M., Cárdenas Domínguez, J. L., Corral-Rivas, J. J., Jiménez, E., López-Sánchez, C. A., and Vega-Nieva, D. J. 2019. Modeling of Aboveground Biomass with Landsat 8 OLI and Machine Learning in Temperate Forests. *Forests* 11 (1): 11.

Loumou A. and Giourga, C. 2003. Olive groves: The life and identity of the Mediterranean. *Agriculture and Human Values* 20: 87–95.

Loumou, A., Giourga, C., Dimitrakopoulos, P., and Koukoulas, S. 2000. PROFILE: tourism contribution to agro-ecosystems conservation: the case of Lesbos Island, Greece. *Environmental Management* 26 (4): 363-370.

Lu, D. 2006. The potential and challenge of remote sensing-based biomass estimation. *International Journal of Remote Sensing* 27 (7): 1297–1328.

Lu, D., Chen, Q., Wang, G., Liu, L., Li, G., and Moran, E. 2014. A survey of remote sensing-based aboveground biomass estimation methods in forest ecosystems. *International Journal of Digital Earth* 9 (1): 63–105.

Maia Araújo, T., Higuchi, N., and Carvalho, A. 1999. Comparison of formulae for biomass content determination in a tropical rainforest site in the state of Pará, Brazil. *Forest Ecology and Management* 117 (1-3): 43–52.

Matzdorf, B. and Meyer, C. 2014. The relevance of the ecosystem services framework for developed countries' environmental policies: A comparative case study of the US and EU. *Land Use Policy 38*: 509–521.

Mauya, E. W., Koskinen, J., Tegel, K., Hämäläinen, J., Kauranne, T., and Käyhkö, N. 2019. Modelling and Predicting the Growing Stock Volume in Small-Scale Plantation Forests of Tanzania Using Multi-Sensor Image Synergy. *Forests* 10 (3): 279.

Michalopoulos, G., Kasapi, K. A., Koubouris, G., Psarras, G., Arampatzis, G., Hatzigiannakis, E., and Kokkinos, G. 2020. Adaptation of Mediterranean Olive Groves to Climate Change through Sustainable Cultivation Practices. *Climate* 8 (4): 54.

Moreira, F., Herrera, J., and Beja, P. 2019. Making olive oil sustainable. *Science* 365 (6456): 873-875.

Morugán-Coronado, A., Linares, C., Gómez-López, M., Faz, Á. and Zornoza, R. 2020. The impact of intercropping, tillage and fertilizer type on soil and crop yield in fruit orchards under Mediterranean conditions: A meta-analysis of field studies. *Agricultural Systems* 178 (10): 27-36.

Mutanga, O. and Skidmore, A. K. 2004. Narrow band vegetation indices overcome the saturation problem in biomass estimation. *International Journal of Remote Sensing* 25 (19): 3999-4014.

Nair, R., Mehta, C. and Sharma, S. 2015. Carbon sequestration in soils. *Agricultural Reviews* 36 (2): 81.

Neves, B., and Pires, I. M. 2018. The Mediterranean diet and the increasing demand of the olive oil Sector: shifts and environmental consequences. *Region* 5 (1): 101–112.

Nguyen, T. D. and Kappas, M. 2020. Estimating the Aboveground Biomass of an evergreen broadleaf forest in Xuan Lien Nature Reserve, Thanh Hoa, Vietnam, using SPOT-6 data and the Random Forest Algorithm. *International Journal of Forestry Research* 2020: 1–13.

Njana, M. A., Bollandsås, O. M., Eid, T., Zahabu, E., and Malimbwi, R. E. 2015. Above- and belowground tree biomass models for three mangrove species in Tanzania: a nonlinear mixed effects modelling approach. *Annals of Forest Science* 73 (2): 353–369.

NSSG. 2005. Agriculture Statistics of Greece. Piraeus: National Statistical Service of Greece. Accessed March 13. URL: https://www.statistics.gr/en/home/

OPEKEPE. 2021. The Greek Payment Authority of Common Agricultural Policy (C.A.P.). Accessed May 13. URL: www.opekepe.gr website: https://www.opekepe.gr/en/

Orlandi, F., Garcia-Mozo, H., Galán, C., Romano, B., de la Guardia, C. D., Ruiz, L., del Mar Trigo, M., Dominguez-Vilches, E., and Fornaciari, M. 2010. Olive flowering trends in a large Mediterranean area (Italy and Spain). *International Journal of Biometeorology* 54: 151–163.

Ozdemir, Y. 2016. Effects of climate change on olive cultivation and table olive and olive oil quality. *Scientific Papers: Horticulture* 60 (B).

Pandit, S., Tsuyuki, S., and Dube, T. 2018. Estimating Above-Ground Biomass in Sub-Tropical Buffer Zone Community Forests, Nepal, Using Sentinel 2 Data. *Remote Sensing* 10 (4): 601.

Panozzo, A., Bernazeau, B. and Desclaux, D. 2019. Durum wheat in organic olive orchard: good deal for the farmers? *Agroforestry Systems* 94 (3): 707-717.

Papanastasis, V. P., Mantzanas K., Dini-Papanastasi O., and Ispikoudis, I. 2009. Traditional agroforestry systems and their evolution in Greece. In agroforestry in Europe. Current Status and future prospects, eds. A. Rigueiro-Rodróguez, J. Mcadam, and M.R. Mosquera-Losada. *Springer: Science* 89-109.

Pilgrim, M. and Willison, S. 2009. Dive Into Python 3. *Springer* 2.

Poley, L. and McDermid, G. 2020. A systematic review of the factors influencing the estimation of vegetation aboveground biomass using unmanned aerial systems. *Remote Sensing* 12 (7): 1052.

Polykretis, C., Grillakis, M. G., and Alexakis, D. D. 2020. Exploring the impact of various spectral indices on land cover change detection using change vector analysis: a case study of Crete island, Greece. *Remote Sensing* 12(2): 319.

Potapov, P., Li, X., Hernandez-Serna, A., Tyukavina, A., Hansen, M. C., Kommareddy, A., and Hofton, M. 2021. Mapping global forest canopy height through integration of GEDI and Landsat data. *Remote Sensing of Environment* 253 112-165.

Poudel, K. P. and Temesgen, H. 2016. Methods for estimating aboveground biomass and its components for Douglas-fir and lodgepole pine trees. *Canadian Journal of Forest Research* 46 (1) 77–87.

Prabhakara, K., Hively, W. D., and McCarty, G. W. 2015. Evaluating the relationship between biomass, percent groundcover and remote sensing indices across six winter cover crop fields in Maryland, United States. *International Journal of Applied Earth Observation and Geoinformation* 39, 88–102.

Puletti, N., Grotti, M., Ferrara, C., and Chianucci, F. 2020. Lidar-based estimates of aboveground biomass through ground, aerial, and satellite observation: a case study in a Mediterranean forest. *Journal of Applied Remote Sensing* 14 (4).

Quijas, S., Boit, A., Thonicke, K., Murray-Tortarolo, G., Mwampamba, T., Skutsch, M., … Balvanera, P. 2018. Modelling carbon stock and carbon sequestration ecosystem services for policy design: a comprehensive approach using a dynamic vegetation model. *Ecosystems and People* 15(1) 42–60.

Rashid, R. and Seizov, P. 2012. *Assessment of carbon stocks as an ecosystem service at Rusenski Lom Nature Park*. The World Wide Fund for Nature (WWF). Accessed April 18. URL: https://d2ouvy59p0dg6k.cloudfront.net/downloads/wwf_rusenski_lom_report_english.pdf

Ravindranath, N. H. and Ostwald, M. 2008. Carbon inventory methods: handbook for greenhouse gas inventory, carbon mitigation and roundwood production projects. Dordrecht: Springer. Accessed May 1. URL: https://www.springer.com/gp/book/9781402065460

R Core Team. 2014. R: A language and environment for statistical computing. R Foundation for Statistical Computing. Vienna: Austria. Accessed February 26. URL: https://www.gbif.org/ru/tool/81287/r-a-language-and-environment-for-statistical-computing

Robertson, G. P. 2000. Greenhouse gases in intensive agriculture: contributions of individual gases to the radiative forcing of the atmosphere. *Science 289* (5486): 1922–1925.

Rosenqvist, Å., Milne, A., Lucas, R., Imhoff, M., and Dobson, C. 2003. A review of remote sensing technology in support of the Kyoto Protocol. *Environmental Science & Policy* 6 (5): 441–455.

Russo, C., Cappelletti, G., Nicoletti, G., Di Noia, A., and Michalopoulos, G. 2016. Comparison of European olive production systems. *Sustainability* 8 (8): 825.

Saarela, S., Grafström, A., Ståhl, G., Kangas, A., Holopainen, M., Tuominen, S., … Hyyppä, J. 2015. Model-assisted estimation of growing stock volume using different combinations of LIDAR and Landsat data as auxiliary information. *Remote Sensing of Environment* 158: 431–440.

Santoro, M., Beer, C., Cartus, O., Schmullius, C., Shvidenko, A., McCallum, I., … Wiesmann, A. 2011. Retrieval of growing stock volume in boreal forest using hyper-temporal series of Envisat ASAR ScanSAR backscatter measurements. *Remote Sensing of Environment* 115 (2): 490–507.

Scheidel, A. and Krausmann, F. 2011. Diet, trade and land use: a socio-ecological analysis of the transformation of the olive oil system. *Land Use Policy 2*8 (1): 47–56.

Silva, C. A., Duncanson, L., Hancock, S., Neuenschwander, A., Thomas, N., Hofton, M., … Dubayah, R. 2021. Fusing simulated GEDI, ICESat-2 and NISAR data for regional aboveground biomass mapping. *Remote Sensing of Environment* 253: 112-234.

Sofo, A., Dichio, B., Xiloyannis, C., and Masia, A. 2004. Lipoxygenase activity and proline accumulation in leaves and roots of olive trees in response to drought stress. *Physiologia Plantarum* 121 (1): 58–65.

Sofo, A., Nuzzo, V., Palese, A. M., Xiloyannis, C., Celano, G., Zukowskyj, P., and Dichio, B. 2005. Net CO2 storage in mediterranean olive and peach orchards. *Scientia Horticulturae* 107 (1): 17–24.

Solomou, A. and Sfougaris, A. 2011. Comparing Conventional and Organic Olive Groves in Central Greece: Plant and Bird Diversity and Abundance. *Renewable Agriculture and Food Systems* 26 (4): 297–316.

Srivastava, P., Kumar, A., Behera, S., Sharma, Y., and Singh, N. 2012. Soil carbon sequestration: an innovative strategy for reducing atmospheric carbon dioxide concentration. *Biodiversity and Conservation* 21 (5): 1343-1358.

Tallis, H., Kareiva, P., Marvier, M., and Chang, A. 2008. An ecosystem services framework to support both practical conservation and economic development. *Proceedings of the National Academy of Sciences* 105 (28): 9457–9464.

Tang, H. and Armston, J. 2019. Algorithm Theoretical Basis Document (ATBD) for GEDI L2B Footprint Canopy Cover and Vertical Profile Metrics. Goddard Space Flight Center. Accessed February 24. URL: https://lpdaac.usgs.gov/documents/588/GEDI_FCCVPM_ATBD_v1.0.pdf

Tang, H., Dubayah, R., Swatantran, A., Hofton, M., Sheldon, S., Clark, D. B., and Blair, B. 2012. Retrieval of vertical LAI profiles over tropical rain forests using waveform lidar at La Selva, Costa Rica. *Remote Sensing of Environment* 124: 242–250.

Tartaglini, N., Calabrese, G., and Servadei, L. 2012. Ancient olive orchards as high nature value farmland: a shared vision at Euro-Mediterranean level. In A multi-scale and multi-level approach for conservation of ancient olive orchards in the Euro-Mediterran Region: 27-42.

The United Nations Development Programme (UNDP). (2019). NDC Global Outlook Report 2019. Retrieved March 11, 2021, from UNDP website: https://www.undp.org/content/undp/en/home/librarypage/environment-energy/climate_change/ndc-global-outlook-report-2019.html

The United Nations Framework Convention on Climate Change (UNFCCC). 1998. Kyoto Protocol to the UNFCCC. Accessed April 22. URL: from https://unfccc.int/resource/docs/convkp/kpeng.pdf

_____. 2015. Adoption of the Paris Agreement. Accessed April 20. URL: https://unfccc.int/sites/default/files/english_paris_agreement.pdf

_____. 2021. Nationally determined contributions under the Paris Agreement. Synthesis report by the secretariat. Accessed April 20. URL: https://unfccc.int/sites/default/files/resource/cma2021_02_adv.pdf

Treuhaft, R. N., Gonçalves, F. G., Drake, J. B., Chapman, B. D., dos Santos, J. R., Dutra, L. V., and Purcell, G. H. 2010. Biomass estimation in a tropical wet forest using Fourier transforms of profiles from lidar or interferometric SAR. *Geophysical Research Letters 37* (23).

United States Environmental Protection Agency (US EPA). 2020. Sources of Greenhouse Gas Emissions. Accessed March 1. URL: https://www.epa.gov/ghgemissions/sources-greenhouse-gas-emissions

United States Geological Survey (USGS). 2016. What are the best Landsat spectral bands for use in my research? Accessed April 12. URL: https://www.usgs.gov/faqs/what-are-best-landsat-spectral-bands-use-my-research?qt-news_science_products=0#qt-news_science_products

_____. 2021. EarthExplorer satellite images database. Accessed May 12. URL: https://earthexplorer.usgs.gov/

Veenendaal, E. M., Torello-Raventos, M., Feldpausch, T. R., Domingues, T. F., Gerard, F., Schrodt, F., … Villarroel, D. 2015. Structural, physiognomic and above-ground biomass variation in savanna–forest transition zones on three continents – how different are co-occurring savanna and forest formations? *Biogeosciences* 12 (10): 2927–2951.

Vossen, P. 2006. Olive oil yield factors affecting production. Newsletter of olive oil production and evaluation. *University of California Cooperative Extension* 2 (1).

Wang, Y. and Fang, H. 2020. Estimation of LAI with the LIDAR technology: a review. *Remote Sensing* 12 (20): 3457.

Woldemariam, T. 2015. GHG emission assessment guideline volume II: Aboveground biomass field guide for baseline survey. Federal Democratic Republic of Ethiopia, Ministry of Agriculture Addis Ababa Ethiopia. Accessed May 24. URL:

https://ghgprotocol.org/sites/default/files/standards_supporting/GHG%20Assessment%20Guideline%20Volume%20II%20Aboveground%20Biomass_0.pdf

Zagaria, C., Schulp, C. J. E., Kizos, T., Gounaridis, D., and Verburg, P. H. 2017. Cultural landscapes and behavioral transformations: An agent-based model for the simulation and discussion of alternative landscape futures in East Lesvos, Greece. *Land Use Policy* 65: 26–44.

Appendices

Appendix I. Python script for retrieving GEDI L2B data with vertical profiles

```
import os
import h5py
import numpy as np
import pandas as pd
import geopandas as gp
from shapely.geometry import Point
import sys
import datetime

QualityCheck = True
QualityFlag = 1
SensitivityCheck = True
SensitivityThreshold = 0.95
CoverNoDataCheck = True
PAINoDataCheck = True
NoDataValue = -9999

CalculateVegetationHeight = True
RetrieveVerticalProfile = True

WorkingDir = "/Users/elenapalenova/Desktop/GIS/GEDI"
inDir = WorkingDir + "/GEDI_All_Files"
inVectorDir = WorkingDir + "/Vector_Data"
outDir = WorkingDir + "/Results/Vector"

gediFiles = [g for g in os.listdir(inDir) if g.startswith('GEDI02_B') and g.endswith('.h5')] # List all GEDI L2B .h5 files in inDir

Coastline_gdf = gp.read_file(inVectorDir + "/Coastline_EGSA87.shp")

Lesvos_Points_EGSA_DF = pd.DataFrame(columns=['Beam', 'ShotNm', 'Long', 'Lat', 'Elev', 'Quality', 'Sens', 'Height', 'Cover', 'PAI', "Date", "Time"])
```

```
for H5File in gediFiles:
    theYear = H5File[9:13]
    theDayOfYear = H5File[13:16]
    theTime = H5File[16:22]

    theDate = str(datetime.date(int(theYear), 1, 1) + datetime.timedelta(int(theDayOfYear) - 1))
    theDate = theDate[-2:] + "/" + theDate[5:7] + "/" + theYear
    theTime = theTime[:2] + ":" + theTime[2:4] + ":" + theTime[-2:]

    gediL2B = h5py.File(inDir + "/" + H5File, 'r')
    H5_Keys = list(gediL2B.keys())
    H5_Metadata = list(gediL2B['METADATA'])

    beamNames = [g for g in gediL2B.keys() if g.startswith('BEAM')]

    gediL2B_objs = []
    gediL2B.visit(gediL2B_objs.append)
    gediSDS = [o for o in gediL2B_objs if isinstance(gediL2B[o], h5py.Dataset)]
    [i for i in gediSDS if beamNames[0] in i][0:10]

    Longitudes, Latitudes, Elevation, Shots, Quality, Beam = [], [], [], [], [], []

    Lesvos_Points_DF = pd.DataFrame(columns=['Beam', 'ShotNm', 'Long', 'Lat', 'Elev', 'Quality', 'Sens', 'Height',
'Cover', 'PAI', "Date", "Time"])
    Points_DF = pd.DataFrame(columns=['Beam', 'ShotNm', 'Long', 'Lat', 'Elev', 'Quality', 'Sens', 'Height', 'Cover',
'Cover_Z', 'PAI', "Date", "Time"])

    print("Reading Data for " + theDate)
    i = 0
    for b in beamNames:

        dZ = gediL2B[b + '/ancillary/dz']

        Latitudes = gediL2B[b + '/geolocation/lat_lowestmode']
        Longitudes = gediL2B[b + '/geolocation/lon_lowestmode']
        Elevations = gediL2B[b + '/geolocation/elev_lowestmode']
        Shots = gediL2B[b + '/geolocation/shot_number']

        Quality = gediL2B[b + '/l2b_quality_flag']
```

```
    Sensitivity = gediL2B[b + '/sensitivity']

    Cover = gediL2B[b + '/cover']
    Cover_z = gediL2B[b + '/cover_z']
    PAI = gediL2B[b + '/pai']

    RH100 = gediL2B[b + '/rh100']

    print(b, dZ[0])

    Points_DF = pd.DataFrame({'Beam': beamNames[i], 'ShotNm': Shots, 'Long': Longitudes, 'Lat': Latitudes, 'Elev': Elevations,
                              'Quality': Quality, 'Sens': Sensitivity, 'Height': 0, 'Cover': Cover , 'Cover_Z': Cover_z , 'PAI': PAI, "Date": theDate, "Time": theTime,
                              "RH100": RH100})

    PointsCount = len(Points_DF)
    print("Found Total " + str(PointsCount) + " Points")

    Spatial_Selection_DF = (Points_DF[((Points_DF["Long"] > 25.8) & (Points_DF["Long"] < 26.7)) & ((Points_DF["Lat"] > 38.9) & (Points_DF["Lat"] < 39.4))])
    print("Removed " + str(PointsCount - len(Spatial_Selection_DF)) + " Points Outside Study Area")
    PointsCount = len(Spatial_Selection_DF)

    if (QualityCheck == True):
        Spatial_Selection_DF = Spatial_Selection_DF[Spatial_Selection_DF["Quality"] == QualityFlag]
        print("Removed " + str(PointsCount - len(Spatial_Selection_DF)) + " Points from QualityFlag")
        PointsCount = len(Spatial_Selection_DF)
    if (SensitivityCheck == True):
        Spatial_Selection_DF = Spatial_Selection_DF[Spatial_Selection_DF["Sens"] >= SensitivityThreshold]
        print("Removed " + str(PointsCount - len(Spatial_Selection_DF)) + " Points from Sensitivity Flag")
        PointsCount = len(Spatial_Selection_DF)
    if (CoverNoDataCheck == True):
        Spatial_Selection_DF = Spatial_Selection_DF[Spatial_Selection_DF["Cover"] != NoDataValue]
        print("Removed " + str(PointsCount - len(Spatial_Selection_DF)) + " Points Having Cover NoData Values")
        PointsCount = len(Spatial_Selection_DF)
    if (PAINoDataCheck == True):
        Spatial_Selection_DF = Spatial_Selection_DF[Spatial_Selection_DF["PAI"] != NoDataValue]
        print("Removed " + str(PointsCount - len(Spatial_Selection_DF)) + " Points Having PAI NoData Values")
```

```
            PointsCount = len(Spatial_Selection_DF)

        print("Found " + str(len(Spatial_Selection_DF)) + " Points for " + b)
        print()

        if (len(Spatial_Selection_DF) > 0):

            VegetationHeight = []
            if CalculateVegetationHeight == True:
                TotalBeamPoints = 0
                for BeamPointID in range(0,len(Spatial_Selection_DF)):
                    BeamPoint = Spatial_Selection_DF.iloc[BeamPointID, Spatial_Selection_DF.columns.get_loc('Cover_Z')]
                    BeamPointHeight = (len(BeamPoint) - BeamPoint.count(0)) * dZ[0]
                    Spatial_Selection_DF.iloc[BeamPointID, Spatial_Selection_DF.columns.get_loc('Height')] = BeamPointHeight
                    TotalBeamPoints = TotalBeamPoints + 1

            Spatial_Selection_DF = Spatial_Selection_DF.drop(columns=['Cover_Z'])
            Lesvos_Points_DF = Lesvos_Points_DF.append(Spatial_Selection_DF, ignore_index=True)
            i += 1
    print("Reading Completed")

    geometry = [Point(xyz) for xyz in zip(Lesvos_Points_DF['Long'], Lesvos_Points_DF['Lat'], Lesvos_Points_DF['Elev'])]
    crs_WGS84 = 'epsg:4326'
    gdf_WGS84 = gp.GeoDataFrame(Lesvos_Points_DF, crs=crs_WGS84, geometry = geometry)

    crs_EGSA87 = 'epsg:2100'
    gdf_EGSA87 = gdf_WGS84.to_crs(crs_EGSA87)

    gdf_EGSA87_Masked = gp.clip(gdf_EGSA87, Coastline_gdf)

    Lesvos_Points_EGSA_DF = Lesvos_Points_EGSA_DF.append(gdf_EGSA87_Masked, ignore_index=True)

    print("Found Total " + str(len(gdf_EGSA87_Masked)) + " Points for " +  theDate)
    print()

if (len(Lesvos_Points_EGSA_DF) > 0):
    print("Exporting GEDI Data to Shapefile....")
```

```
    geometry = [Point(xyz) for xyz in zip(Lesvos_Points_EGSA_DF['Long'], Lesvos_Points_EGSA_DF['Lat'],
Lesvos_Points_EGSA_DF['Elev'])]
    crs_WGS84 = 'epsg:4326'
    gdf_WGS84 = gp.GeoDataFrame(Lesvos_Points_EGSA_DF, crs=crs_WGS84, geometry = geometry)
    crs_EGSA87 = 'epsg:2100'
    gdf_EGSA87 = gdf_WGS84.to_crs(crs_EGSA87)

    gdf_EGSA87.to_file(driver="ESRI Shapefile", filename = outDir + "/Points_EGSA87_Vertical_Profile.shp")
```

Appendix II. Python script for Creating Fishnet for Lesvos island

```
import arcpy
from arcpy import env

inFC = arcpy.GetParameterAsText(0)
CS = int(arcpy.GetParameterAsText(1))
OutFC = arcpy.GetParameterAsText(2)

desc = arcpy.Describe(inFC)
inSRS = desc.spatialReference

theExtent = desc.Extent
theXmin = theExtent.XMin
theNewXmin = int(theXmin / CS) * CS
theYmin = theExtent.YMin
theNewYmin = int(theYmin / CS) * CS

theXmax = theExtent.XMax
theNewXmax = (int(theXmax / CS) + 1) * CS
theYmax = theExtent.YMax
theNewYmax = (int(theYmax / CS) + 1) * CS

print(theNewXmin, theNewYmin, theNewXmax, theNewYmax)

arcpy.Delete_management(OutFC)

originCoordinate = str(theNewXmin) + " " + str(theNewYmin)
yAxisCoordinate = str(theNewXmin) + " " + str(theNewYmin + CS)
```

```
oppositeCoorner = str(theNewXmax) + " " + str(theNewYmax)

numRows = "#"
numColumns  = "#"

labels = "NO_LABELS"
templateExtent = '#'
geometryType = 'POLYGON'

arcpy.CreateFishnet_management(OutFC, originCoordinate, yAxisCoordinate, str(CS), str(CS), numRows, numColumns, oppositeCoorner, labels, templateExtent, geometryType)

arcpy.DefineProjection_management(OutFC, inSRS)

Fishnet = arcpy.MakeFeatureLayer_management(OutFC, "Fishnet")

arcpy.SetParameter(3, Fishnet)
```

Appendix III. Python script for selecting random sampling points

```
import arcpy
import numpy as np
import random
from arcpy import env
import sys
import math

Points_Count = 20
CoverThreshold = 70

theCombinedRsterFN = "/Users/elenapalenova/Desktop/GIS/GEDI/Sampling_Model/Results/Combined.img"
theCombinedRster = arcpy.RasterToNumPyArray(theCombinedRsterFN, nodata_to_value=-9999)

theGeographical_DistributionFN = "/Users/elenapalenova/Desktop/GIS/GEDI/Sampling_Model/Results/Geographical_Distribution.img"
theGeographical_DistributionRsterArray = arcpy.RasterToNumPyArray(theGeographical_DistributionFN, nodata_to_value=-9999)
```

```
theGeographical_DistributionRsterUV_List = np.unique(theGeographical_DistributionRsterArray)
theGeographical_DistributionRster = arcpy.Raster(theGeographical_DistributionFN)

theMaskFN = "/Users/elenapalenova/Desktop/GIS/GEDI/Sampling_Model/Results/Mask.img"
theMaskRsterArray = arcpy.RasterToNumPyArray(theMaskFN, nodata_to_value=-9999)

Region_List = []
Percentage_List = []
for r in arcpy.SearchCursor(theGeographical_DistributionRster, "", "", "VALUE; Region; Percentage"):
    Region_List.append(r.getValue("Region"))
    Percentage_List.append(r.getValue("Percentage"))

desc = arcpy.Describe(theCombinedRsterFN)
inSRS = desc.spatialReference

theXminimum = desc.extent.XMin
theXmaximum = desc.extent.XMax
theYminimum = desc.extent.YMin
theYmaximum = desc.extent.YMax

CS = desc.meanCellWidth

NoDataValue = desc.noDataValue

theCombinedRster = np.where(theCombinedRster != NoDataValue, theCombinedRster, -9999)

theCombinedRster = np.where(theMaskRsterArray >= CoverThreshold, theCombinedRster, -9999)

theCombinedRasterUV_List = np.unique(theCombinedRster)

out_path = "/Users/elenapalenova/Desktop/GIS/GEDI/Sampling_Model/Results/"
out_name = "Random_Points.shp"
geometry_type = "POINT"
template = ""
has_m = "DISABLED"
has_z = "DISABLED"

arcpy.Delete_management(out_path + "\\" + out_name)
fc = arcpy.CreateFeatureclass_management(out_path, out_name, geometry_type, template, has_m, has_z, inSRS)
arcpy.AddField_management(fc, "Region", "TEXT", "", "", "20")
```

```
arcpy.AddField_management(fc, "Type", "TEXT", "", "", "5")

#cursor = arcpy.da.InsertCursor(fc, ["SHAPE@"])
cursor = arcpy.da.InsertCursor(fc, ["SHAPE@", "Region", "Type"])

Points_Dir = {}
for Region_index in range(1, len(theGeographical_DistributionRsterUV_List)):

   theRegion_Raster = np.where((theCombinedRster != NoDataValue) & (theGeographical_DistributionRsterArray == theGeographical_DistributionRsterUV_List[Region_index]), theCombinedRster, -9999)
   Region_Points_Count =  Points_Count * Percentage_List[Region_index-1] / 100
   print(Region_Points_Count)
   Region_Points_Dir = {}

   for i in range(1, len(theCombinedRasterUV_List)):

      points = []
      points_coordinates = []
      c = np.where((theRegion_Raster != NoDataValue) & (theRegion_Raster == theCombinedRasterUV_List[i]))
      X = c[0].tolist() # x list
      Y = c[1].tolist() # y list

      if (len(X) != 0):
         while(len(points) < Region_Points_Count):

            row= random.choice(X) # choose random point from class n
            ind = X.index(row) # find location of this point
            col = Y[ind] # find corresponding y point
            points.append((row, col)) # add to points list

            XCoordinate = theXminimum + (col * CS) + (CS/2)
            YCoordinate = theYmaximum - (row * CS) - (CS/2)
            points_coordinates.append((XCoordinate, YCoordinate))
            cursor.insertRow([arcpy.Point(XCoordinate, YCoordinate), Region_List[Region_index-1], theCombinedRasterUV_List[i]])

      Region_Points_Dir[theCombinedRasterUV_List[i]] = points_coordinates
   Points_Dir[Region_List[Region_index-1]] = Region_Points_Dir
```

Appendix IV. Python script for creating VI from Satellite Images bands

```
from osgeo import gdal
import numpy as np
import os
import sys
import math

def array2raster(newRasterfn,rasterOrigin,pixelWidth,pixelHeight,inSRS_wkt,array,Pixel_Type,NoDataValue):
    cols = array.shape[1]
    rows = array.shape[0]
    originX = rasterOrigin[0]
    originY = rasterOrigin[1]
    driver = gdal.GetDriverByName('GTiff')
    outRaster = driver.Create(newRasterfn, cols, rows, 1, Pixel_Type)
    outRaster.SetGeoTransform((originX, pixelWidth, 0, originY, 0, pixelHeight))
    outband = outRaster.GetRasterBand(1)
    outband.WriteArray(array[::-1])
    outband.SetNoDataValue(NoDataValue)
    outRaster.SetProjection(inSRS_wkt)
    outband.FlushCache()

def NDVI_calculation(theNoDataValue, Red_array, NIR_array):
    NDVI_array_calculation = np.where((Red_array != theNoDataValue) & (NIR_array != theNoDataValue), (NIR_array - Red_array) / (NIR_array + Red_array), theNoDataValue)
    return NDVI_array_calculation

def TVI_calculation(theNoDataValue, Red_array, NIR_array):
    No_Data_Array = np.where((Red_array != theNoDataValue) &  (NIR_array != theNoDataValue) , 1, theNoDataValue)
    Negative_Values_Array = np.where(((NIR_array - Red_array) / (NIR_array + Red_array)) + 0.5  >= 0, (((NIR_array - Red_array) / (NIR_array + Red_array)) + 0.5), -theNoDataValue)
    Boolean_Array = np.where((No_Data_Array != theNoDataValue) & (Negative_Values_Array != -theNoDataValue), 1, -theNoDataValue)
    TVI_array_calculation = np.where(Boolean_Array != -theNoDataValue,  (Negative_Values_Array ** 0.5) * 100, theNoDataValue)
    return TVI_array_calculation
```

```
def EVI_calculation(theNoDataValue, Blue_array, Red_array, NIR_array):
    No_Data_Array = np.where((Blue_array != theNoDataValue) &  (Red_array != theNoDataValue) & (NIR_array != theNoDataValue), 1, theNoDataValue)
    Zero_Values_Array = np.where((NIR_array + (6 * Red_array) - (7.5 * Blue_array) + 1)  != 0, (NIR_array + (6 * Red_array) - (7.5 * Blue_array) + 1), theNoDataValue)
    Boolean_Array = np.where((No_Data_Array != theNoDataValue) & (Zero_Values_Array != theNoDataValue), 1, theNoDataValue)
    EVI_array_calculation = np.where(Boolean_Array != theNoDataValue, 2.5 * ((NIR_array - Red_array) / Zero_Values_Array), theNoDataValue)
    return EVI_array_calculation

def SAVI_calculation(theNoDataValue, Red_array, NIR_array):
    SAVI_array_calculation = np.where((Red_array != theNoDataValue) &  (NIR_array != theNoDataValue), ((NIR_array - Red_array) / (NIR_array + Red_array + 0.5)) * (1.5), theNoDataValue)
    return SAVI_array_calculation

def MSAVI_calculation(theNoDataValue, Red_array, NIR_array):
    No_Data_Array = np.where((Red_array != theNoDataValue) & (NIR_array != theNoDataValue) , 1, theNoDataValue)
    Negative_Values_Array = np.where((np.sqrt((2 * NIR_array + 1) ** 2 - 8 * (NIR_array - Red_array)) < 0, np.sqrt((2 * NIR_array + 1) ** 2 - 8 * (NIR_array - Red_array)), theNoDataValue)
    Boolean_Array = np.where(((No_Data_Array != theNoDataValue) & (Negative_Values_Array != -theNoDataValue)), 1, -theNoDataValue)
    MSAVI_array_calculation = np.where(Boolean_Array != -theNoDataValue, (2 * NIR_array + 1 - Negative_Values_Array), theNoDataValue)
    return MSAVI_array_calculation

def export_indices(output_folder, NDVI_array, TVI_array, EVI_array, SAVI_array, MSAVI_array):
    filename = os.path.expanduser(output_folder + "/NDVI.TIF")
    array2raster(filename,(originx,originy),xres,xres,inSRS_wkt,NDVI_array, gdal.GDT_Float32,-9999)

    filename = os.path.expanduser(output_folder + "/TVI.TIF")
    array2raster(filename,(originx,originy),xres,xres,inSRS_wkt,TVI_array, gdal.GDT_Float32,-9999)

    filename = os.path.expanduser(output_folder + "/EVI.TIF")
    array2raster(filename,(originx,originy),xres,xres,inSRS_wkt,EVI_array, gdal.GDT_Float32,-9999)

    filename = os.path.expanduser(output_folder + "/SAVI.TIF")
    array2raster(filename,(originx,originy),xres,xres,inSRS_wkt,MIRBI_array, gdal.GDT_Float32,-9999)
```

```
    filename = os.path.expanduser(output_folder + "/MSAVI.TIF")
    array2raster(filename,(originx,originy),xres,xres,inSRS_wkt,MIRBI_array, gdal.GDT_Float32,-9999)

satellite_sensor = "Landsat8"

input_satellite_data_folder =
os.path.expanduser("/Users/elenapalenova/Desktop/GIS/Indices/Input_Satellite_Images")

if satellite_sensor == "Landsat8":
    the_output_folder = "~/Desktop/GIS/Indices/Results/Indices/Landsat8/"
else:
    print("Code must be updated")

subfolders = os.listdir(input_satellite_data_folder)
for folder in subfolders:
    if satellite_sensor == "Landsat8":
        if folder[:4] == "LC08":
            acquisition_date = folder[17:25]

            date = acquisition_date[-2:] + "_" + acquisition_date [4:6] + "_" + acquisition_date[:4]
            header_file = folder + "_MTL.txt"
            header_file_path = input_satellite_data_folder + "/" + folder + "/" + header_file

            f = open(header_file_path, "r")

            lines = f.readlines()
            count = 0

            for line in lines:
                acquired_bool = line[4:17]
                if acquired_bool == "DATE_ACQUIRED":
                    line_date = line[-3:-1] + "_" + line[-6:-4] + "_" + line[-11:-7]
                    break

            B2_file_path = input_satellite_data_folder + "/" + folder + "/" + folder + "_SR_B2.TIF"
            B2 = os.path.expanduser(B2_file_path)
            #blue

            B4_file_path = input_satellite_data_folder + "/" + folder + "/" + folder + "_SR_B4.TIF"
            B4 = os.path.expanduser(B4_file_path)
```

```
#red

B5_file_path = input_satellite_data_folder + "/" + folder + "/" + folder + "_SR_B5.TIF"
B5 = os.path.expanduser(B5_file_path)
#NIR

B6_file_path = input_satellite_data_folder + "/" + folder + "/" + folder + "_SR_B6.TIF"
B6 = os.path.expanduser(B6_file_path)
#SWIR1 or sSWIR

B7_file_path = input_satellite_data_folder + "/" + folder + "/" + folder + "_SR_B7.TIF"
B7 = os.path.expanduser(B7_file_path)
#SWIR2 or lSWIR

input_image = gdal.Open(B2)
B2_raster_array = np.array(input_image.GetRasterBand(1).ReadAsArray().astype(np.float32))

input_image = gdal.Open(B4)
B4_raster_array = np.array(input_image.GetRasterBand(1).ReadAsArray().astype(np.float32))

input_image = gdal.Open(B5)
B5_raster_array = np.array(input_image.GetRasterBand(1).ReadAsArray().astype(np.float32))

input_image = gdal.Open(B6)
B6_raster_array = np.array(input_image.GetRasterBand(1).ReadAsArray().astype(np.float32))

input_image = gdal.Open(B7)
B7_raster_array = np.array(input_image.GetRasterBand(1).ReadAsArray().astype(np.float32))

ulx, xres, xskew, uly, yskew, yres  = input_image.GetGeoTransform()

inSRS_wkt = input_image.GetProjection()

In_RASTER_array = B4_raster_array

[rows,cols] = In_RASTER_array.shape    #Matrix shape on rows and cols
rows = len(In_RASTER_array)
columns = len(In_RASTER_array[0])
originx = ulx
originy = uly - (rows*xres)
```

```
NoDataValue = np.float64(input_image.GetRasterBand(1).GetNoDataValue())

B2_NoData = np.where(B2_raster_array != 0, B2_raster_array, -9999)
B4_NoData = np.where(B4_raster_array != 0, B4_raster_array, -9999)
B5_NoData = np.where(B5_raster_array != 0, B5_raster_array, -9999)
B6_NoData = np.where(B6_raster_array != 0, B6_raster_array, -9999)
B7_NoData = np.where(B7_raster_array != 0, B7_raster_array, -9999)

print("Calculating NDVI for " + line_date)
NDVI_array = NDVI_calculation(-9999, B4_NoData, B5_NoData)

print("Calculating TVI for " + line_date)
TVI_array = TVI_calculation(-9999, B4_NoData, B5_NoData)

print("Calculating EVI for " + line_date)
EVI_array = EVI_calculation(-9999, B2_NoData, B4_NoData, B5_NoData)

print("Calculating SAVI for " + line_date)
SAVI_array = SAVI_calculation(-9999, B4_NoData, B5_NoData)

print("Calculating MSAVI for " + line_date)
MSAVI_array = MSAVI_calculation(-9999, B4_NoData, B5_NoData)

new_folder = the_output_folder + line_date
print("Export indices for " + line_date)

if os.path.exists(os.path.expanduser(new_folder)) == False:
   os.makedirs(os.path.expanduser(new_folder))

export_indices(new_folder, NDVI_array, TVI_array, EVI_array, SAVI_array, MSAVI_array)
```

Appendix V. Correlation and regression analysis in R for field and Landsat 8 data

```
library(readxl)
library(raster)
library(rgdal)
library(sp)

wd <- ("/Users/elenapalenova/Desktop/GIS/Fusion")
datawd <- ("/Users/elenapalenova/Desktop/GIS/Indices/Landsat_New_Data_GEDI_points/LC08_L2SP_181033_20190401_20200829_02_T1/")
setwd(datawd)

theDateString = scan(text=basename(datawd), sep="_", what="", quiet=TRUE)[4]
theDate = as.Date(paste0(substr(theDateString, 7, 8), "/", substr(theDateString, 5, 6), "/", substr(theDateString, 1, 4)), format = "%d/%m/%Y")

file_list = list.files(datawd, pattern = "B\\d+.TIF")

band_list <- list()
for (val in file_list){
band = file_list <- paste0(datawd, val)
band_list <- append(band_list, list(band))
}
rasStack = stack(band_list)

my_data <- read_excel(paste0(wd, "/Data/Final_Plot_metadata.xlsx"))

pointCoordinates=my_data[,c("Lon","Lat","AGBt_field")]

coordinates(pointCoordinates) <- c("Lon", "Lat")
proj4string(pointCoordinates) <- CRS("+init=epsg:4326")

CRS.new <- CRS("+init=epsg:32635")
Projected_pointCoordinates <- spTransform(pointCoordinates, CRS.new)

Projected_pointCoordinates_ForDate <- Projected_pointCoordinates[, c("AGBt_field")]
```

```
theCloudImage  = paste0(datawd, list.files(datawd, pattern = "_ST_CDIST"))
CloudStack <- stack(theCloudImage)
CloudDistanceDF <- extract(CloudStack, Projected_pointCoordinates)

colnames(CloudDistanceDF)[1] <- "CloudDistance"
CloudDistanceDF = CloudDistanceDF[ , "CloudDistance"]

Projected_pointCoordinates$CloudDistance = CloudDistanceDF
Projected_pointCoordinates_WithoutClouds <-
Projected_pointCoordinates[Projected_pointCoordinates$CloudDistance > 0, ]

rasValue=extract(rasStack, Projected_pointCoordinates_WithoutClouds)

Field_points_Biomass <- as.data.frame(Projected_pointCoordinates_WithoutClouds[,c("AGBt_field")])
Regression_Data <- as.data.frame(cbind(Field_points_Biomass[,c("AGBt_field")],rasValue))

colnames(Regression_Data)[1] <- "y"
colnames(Regression_Data)[2] <- "x1"
colnames(Regression_Data)[3] <- "x2"
colnames(Regression_Data)[4] <- "x3"
colnames(Regression_Data)[5] <- "x4"
colnames(Regression_Data)[6] <- "x5"
colnames(Regression_Data)[7] <- "x6"
colnames(Regression_Data)[8] <- "x7"
colnames(Regression_Data)[9] <- "x10"

Regression_Data$NDVI = (Regression_Data$x5 - Regression_Data$x4) / (Regression_Data$x5 +
Regression_Data$x4)
Regression_Data$IRVI = Regression_Data$x4 / Regression_Data$x5
Regression_Data$RVI = Regression_Data$x5 / Regression_Data$x4
Regression_Data$GNDVI = (Regression_Data$x5 - Regression_Data$x3) / (Regression_Data$x5 +
Regression_Data$x3)
Regression_Data$SAVI = 1.5 * (Regression_Data$x5 - Regression_Data$x4) / (Regression_Data$x5 +
Regression_Data$x4 + 0.5)
Regression_Data$TVI = 100 * ((Regression_Data$NDVI + 0.5) ^ 0.5)
Regression_Data$EVI = 2.5 * (Regression_Data$x5 - Regression_Data$x4) / (Regression_Data$x5 + (6 *
Regression_Data$x4) - (7.5 * Regression_Data$x2) + 1)

round(cor(Regression_Data), digits = 2)
```

```
plot(Regression_Data$y, Regression_Data$NDVI)
fit <- lm(y ~ x1 + x2 + x3 + x4 + x5 + x6 + x7 + x10 + NDVI, data=Regression_Data)
summary(fit)
```

Appendix VI. Correlation and regression analysis in R for GEDI and Landsat 8 data

```
library(raster)
library(rgdal)
library(sp)
library(math)

wd <- ("/Users/elenapalenova/Desktop/GIS/Fusion")
datawd <- ("/Users/elenapalenova/Desktop/GIS/Indices/Landsat_New_Data_GEDI_points/LC08_L2SP_181033_20190401_20200829_02_T1/")
setwd(datawd)

theDateString = scan(text=basename(datawd), sep="_", what="", quiet=TRUE)[4]
theDate = as.Date(paste0(substr(theDateString, 7, 8), "/", substr(theDateString, 5, 6), "/", substr(theDateString, 1, 4)), format = "%d/%m/%Y")

file_list = list.files(datawd, pattern = "B\\d+.TIF")

band_list <- list()
for (val in file_list){
band = file_list <- paste0(datawd, val)
band_list <- append(band_list, list(band))
}
rasStack = stack(band_list)

my_data <- readOGR("/Users/elenapalenova/Desktop/GIS/Fusion/Data/Final_Points/Final_GEDI_Points.shp", layer="Final_GEDI_Points")

Biomass_DF <- as.data.frame(my_data[,c("Date", "PAI", "Slope", "Elevation")])

Biomass_DF$Slope_Rcl[Biomass_DF$Slope == ">7%"] <- 1
```

```
Biomass_DF$Slope_Rcl[Biomass_DF$Slope == "<7%"] <- 0
Biomass_DF$Elevation_Rcl[Biomass_DF$Elevation == ">200 m"] <- 1
Biomass_DF$Elevation_Rcl[Biomass_DF$Elevation == "<200 m"] <- 0

Biomass_DF$CanArea <- 18.665 + 20.687*Biomass_DF$PAI - 2.364*Biomass_DF$Elevation_Rcl - 5.366*Biomass_DF$Slope_Rcl

Biomass_DF$Ds=36.2457+0.8371*Biomass_DF$CanArea

Biomass_DF$N=(1/900)*exp(3.519229 - 0.013677*Biomass_DF$Ds)
Biomass_DF$AGBt=Biomass_DF$N * (0.125*Biomass_DF$Ds^2.279)

GEDI_points_data = my_data[,c("Date", "AGBt")]

GEDI_points_data@coords <- GEDI_points_data@coords[, 1:2]

CRS.new <- CRS("+init=epsg:32635")

Projected_pointCoordinates <- spTransform(GEDI_points_data[,c("Date", "AGBt")], CRS.new)

Projected_pointCoordinates_ForDate <- (subset(Projected_pointCoordinates, abs(difftime(as.Date(theDate, format = "%d/%m/%Y"), as.Date(Projected_pointCoordinates$Date, format = "%d/%m/%Y"), units = "days")) <= 20, select = c("Date", "AGBt")))

theCloudImage  = paste0(datawd, list.files(datawd, pattern = "_ST_CDIST"))
CloudStack <- stack(theCloudImage)
CloudDistanceDF <- extract(CloudStack, Projected_pointCoordinates_ForDate)

colnames(CloudDistanceDF)[1] <- "CloudDistance"
CloudDistanceDF = CloudDistanceDF[ , "CloudDistance"]
themis = as.data.frame(CloudDistanceDF)

Projected_pointCoordinates_ForDate$CloudDistance = CloudDistanceDF
Projected_pointCoordinates_WithoutClouds <- Projected_pointCoordinates_ForDate[Projected_pointCoordinates_ForDate$CloudDistance > 100, ]

rasValue=extract(rasStack, Projected_pointCoordinates_WithoutClouds)

GEDI_points_Biomass <- as.data.frame(Projected_pointCoordinates_WithoutClouds[,c("Date", "AGBt")])
Regression_Data <- as.data.frame(cbind(GEDI_points_Biomass[,c("AGBt")],rasValue))
```

```
colnames(Regression_Data)[1] <- "y"
colnames(Regression_Data)[2] <- "x1"
colnames(Regression_Data)[3] <- "x2"
colnames(Regression_Data)[4] <- "x3"
colnames(Regression_Data)[5] <- "x4"
colnames(Regression_Data)[6] <- "x5"
colnames(Regression_Data)[7] <- "x6"
colnames(Regression_Data)[8] <- "x7"
colnames(Regression_Data)[9] <- "x10"

Regression_Data$NDVI = (Regression_Data$x5 - Regression_Data$x4) / (Regression_Data$x5 + Regression_Data$x4)
Regression_Data$IRVI = Regression_Data$x4 / Regression_Data$x5
Regression_Data$RVI = Regression_Data$x5 / Regression_Data$x4
Regression_Data$GNDVI = (Regression_Data$x5 - Regression_Data$x3) / (Regression_Data$x5 + Regression_Data$x3)
Regression_Data$SAVI = 1.5 * (Regression_Data$x5 - Regression_Data$x4) / (Regression_Data$x5 + Regression_Data$x4 + 0.5)
Regression_Data$TVI = 100 * ((Regression_Data$NDVI + 0.5) ^ 0.5)
Regression_Data$EVI = 2.5 * (Regression_Data$x5 - Regression_Data$x4) / (Regression_Data$x5 + (6 * Regression_Data$x4) - (7.5 * Regression_Data$x2) + 1)

round(cor(Regression_Data), digits = 2)

plot(Regression_Data$y, Regression_Data$EVI)
fit <- lm(y ~ x1 + x2 + x3 + x4 + x5 + x6 + x7 + x10 + NDVI + IRVI + RVI + GNDVI + SAVI + TVI + EVI, data=Regression_Data)
summary(fit)
```